Role of the ETV5/p38 signaling axis in aggressive thyroid cancer cells

Jerry H Houl[1], Rozita Bagheri-Yarmand[1], Muthusamy Kunnimalaiyaan[1], Paola Miranda Mendez[1], Joseph L Kidd[1], Ali Dadbin[1], Andrea Jurado-Ruiz[1], Parag A Parekh[1], Ying C Henderson[2], Nikhil S Chari[2], Aatish Thennavan[3], Reid T Powell[3], Clifford C Stephan[3], Xiao Zhao[2], Anastasios Maniakas[2], Roza Nurieva[4], Naifa L Busaidy[1], Maria E Cabanillas[1], Ramona Dadu[1], Mark Zafereo[2], Jennifer R Wang[2], Stephen Y Lai[2,5,6], and Marie-Claude Hofmann[1]

1. Department of Endocrine Neoplasia and Hormonal Disorders, The University of Texas MD Anderson Cancer Center, Houston, TX
2. Department of Head and Neck Surgery, The University of Texas MD Anderson Cancer Center, Houston, TX
3. High Throughput Research and Screening Center, Texas A&M Institute of Biosciences and Technology, Houston, TX
4. Department of Immunology, The University of Texas MD Anderson Cancer Center, Houston, TX
5. Department of Molecular and Cellular Biology, The University of Texas MD Anderson Cancer Center, Houston, TX
6. Department of Radiation Oncology, The University of Texas MD Anderson Cancer Center, Houston, TX

Disclosures:
M Zafereo reports research grant funding for clinical trials from Merck, Eli Lilly, and Exelixis.
ME Cabanillas reports research grants funding for clinical trials from Exelixis, Genentech, and Merck. She reports paid consulting by Novartis, Thryv Therapeutics, Bayer, Exelixis, and Eli Lilly.
MC Hofmann reports research funding from Thryv Therapeutics
A Maniakas reports research funding from Thryv Therapeutics and JAZZ Pharmaceuticals

All other authors declare no potential conflicts of interest.

Running title: ETV5/p38 signaling axis in aggressive thyroid cancer cells

Keywords: Anaplastic thyroid cancer, MAPK pathway, p38/MAPK14 pathway, ETV5, TP53

Address for correspondence:

Marie-Claude Hofmann, Ph.D.
Professor
Department of Endocrine Neoplasia &
Hormonal Disorders
Division of Internal Medicine
The University of Texas MD Anderson Cancer Center
6565 MD Anderson Blvd, room Z8.3024
Houston, TX 77030, USA
Email: mhofmann@mdanderson.org

Abstract

Poorly differentiated thyroid cancer (PDTC) and anaplastic thyroid cancer (ATC) patients face a much poorer prognosis compared to those with differentiated thyroid cancers. Around 25% of PDTCs and 35% of ATCs carry the *BRAF*^{V600E} mutation, which constitutively activates the MAPK pathway, a key driver of cell growth. While combining BRAF and MEK inhibitors can shrink tumors, resistance often develops. The exact cause of this resistance remains unclear.

We previously found that in PDTC and ATC cells the *BRAF*^{V600E} mutation is strongly linked to the expression of ETV5, a transcription factor that is downstream of the MAPK pathway. In the current study, we observed a significant association between ETV5 expression and the activation of p38, a central component of the MAPK14 pathway. Upon reduction of ETV5 levels, p38 expression and activation also decreased, along with its upstream regulators MKK3/MKK6. This suggests that the MAPK and p38/MAPK14 pathways are interconnected and that p38 has oncogenic properties in these cancers.

Using high-throughput screening, we established that combining p38 inhibitors with the BRAF inhibitor dabrafenib showed strong synergy *in vitro*, including in cells resistant to dabrafenib and trametinib that had acquired a secondary *TP53* mutation. We then tested this combination in a genetically engineered mouse model (GEMM) of ATC.

Overall, our findings suggest an oncogenic link between the MAPK and p38/MAPK14 pathways and that combining p38 pathway inhibitors with dabrafenib targeted therapy could improve treatment outcomes for aggressive thyroid cancers. However, more specific and effective p38 inhibitors are needed to fully harness this potential.

Introduction

Transformation of thyroid follicular cells is associated with early driver mutations in the *BRAF* or *RAS* genes in papillary thyroid cancers (PTCs) and follicular thyroid cancers (FTCs) (1). The accumulation of additional driver mutations, including mutations in the *TERT* promoter, leads to undifferentiated tumors such as poorly differentiated thyroid carcinoma (PDTC) and anaplastic thyroid carcinoma (ATCs) (2-5). These rare but highly aggressive malignancies are typically associated with a short median overall survival following diagnosis, unless treated with targeted therapy (6,7).

According to our recent study and work from others (3,8), about 25% of PDTCs and 35% of ATCs harbor the $BRAF^{V600E}$ mutation, which causes unrestricted cell proliferation due to constitutive activation of the MAPK signaling cascade (9). The $BRAF^{V600E}$ mutation also synergizes with *TERT* promoter mutations to increase tumor cell proliferation (10,11). Recently, the survival of patients with BRAF-mutated ATC has been significantly prolonged using neoadjuvant targeted therapies that involve a $BRAF^{V600E}$ inhibitor (dabrafenib) in combination with a MEK1/2 inhibitor (trametinib) followed by surgical resection (7,12,13). Further, immunotherapy in combination with kinase inhibitors may provide additional survival benefit (14,15). Despite these advances, tumor progression rates remain high, and many patients die early from PDTC and ATC. The molecular mechanisms driving resistance to treatments are poorly understood, however several resistance pathways have been proposed. These include activation of alternate signaling pathways mediated by PI3K/AKT (16), alternate *BRAF* splicing (17,18), or reactivation of the MAPK pathway by receptors of the ERBB or FGF receptor families (19,20), amongst others. Also, genomic heterogeneity of PDTC/ATC cells under drug treatment may stimulate clonal evolution and the development of more aggressive phenotypes

(21,22). We recently reported that long-term (over 5 months) exposure of PDTC KTC1 cells (*BRAF*^{V600E}) to moderate doses of vemurafenib led to the emergence of new mutations that not only altered the cells morphology but also increased their proliferation rate and triggered protein expression and phosphorylation patterns commonly associated with epithelial-to-mesenchymal transition (16). Interestingly, a distinct subpopulation of these cells developed a *KRAS* mutation (*KRAS*^{G12D}) alongside *BRAF*^{V600E}, giving them a significant advantage in proliferation and invasion—traits reminiscent of ATC. These findings are clinically important, as we later observed acquired *KRAS*^{G12D}, *NRAS*^{Q61K}, and *KRAS*^{G12V} mutations in 50% of *BRAF*^{V600E} PTC and ATC patients during progression on dabrafenib or dabrafenib plus trametinib treatments (23). This highlights a key mechanism in therapy resistance and progression. We and others have also detected acquired secondary mutations in the *TP53*, *PTEN*, *NF1*, *PIK3CA*, and *NF2* genes (24,25), which are tumor suppressor genes that are so far not efficiently targetable.

Effective therapies for patients affected with PDTC or ATC remain an important unmet clinical need that should be addressed because of their susceptibility to progression and poor survival. Unfortunately, few options are available in cases of primary or secondary *RAS* and tumor suppressor mutations. We previously identified the E26 transformation-specific (ETS) transcription factor ETV5 as a downstream target of the RAS/MAPK pathway and confirmed its importance for *BRAF*^{V600E}-mutated PDTC thyroid cancer cell proliferation (26). We also demonstrated its possible role in metastasis due to its ability to drive the expression of *TWIST1*, a known activator of epithelial-to-mesenchymal transition (26).

In the present study, through in silico analysis and pre-clinical models, we identified the stress- and oncokinase p38 (or MAPK14) as a possible downstream target of ETV5. Inhibiting the p38 signaling pathway with pharmacological agents reduced PDTC and ATC tumor cell

growth. One of these compounds, ralimetinib, showed synergy with dabrafenib, particularly in cells that were resistant to dabrafenib/trametinib and harbored a secondary *TP53* mutation. This implies that the mutational status of *TP53* affects the response to p38 inhibitors at progression.

Material and Methods

Cell lines and culture conditions

We used the human thyroid cancer cell lines MDA-T68, MDA-T85, KTC1, KTC1-VA7, Hth83, PDX.008.CL, and SW1736. We also used the mouse ATC cell lines MCH2.2 and PPA6 (Supplementary Table S1). MDA-T68 and MDA-T85 cells were graciously provided by Dr. Stephen Y Lai at the University of Texas MD Anderson Cancer Center (27). The MDA-T68 line was derived from a follicular variant of papillary thyroid carcinoma (FVPTC) with cervical lymph node metastasis. This cell line harbors a $NRAS^{Q61K}$ mutation. The MDA-T85 cell line was derived from a metastatic lymph node in a patient who had a primary PTC with extrathyroidal extension and lympho-vascular invasion. MDA-T85 cells harbor a $BRAF^{V600E}$ and a $HRAS^{Q61K}$ mutations as well as the *TERT* promoter mutation C228T, and they are considered PDTC cells. KTC1 are PDTC cells derived from a metastatic pleural effusion (28) and were kindly provided by Dr. R. Schweppe, University of Colorado, Anschutz Medical Center. These cells harbor the $BRAF^{V600E}$ and the *TERT* promoter C250T mutations (29). KTC1-VA7 is a KTC1 subclone that has spontaneously acquired an additional $KRAS^{G12D}$ mutation after long-term culture with the $BRAF^{V600E}$ inhibitor vemurafenib (16). Hth83 is an ATC cell line established from a giant cell anaplastic thyroid carcinoma (30). Hth83 cells harbor $HRAS^{Q61R}$ as a key genetic driver as well as two frameshifts in the *TP53* gene*:* $TP53^{P153Afs*28}$ and $TP53^{P152fs}$ (29). They also exhibit the *TERT C228T* promoter mutation. SW1736 cells are ATC cells harboring a $BRAF^{V600E}$ mutation,

a *TP53*^{Q192*} truncating mutation, and the *TERT C228T* mutation (29). Hth83 and SW1736 cells were obtained from an established cell line bank in the Department of Head and Neck Surgery at the University of Texas MD Anderson Cancer Center, Houston, TX. The PDX.008.CL cell line was derived from a mediastinal node metastasis of a dabrafenib-resistant human ATC tumor (31). Mouse cell lines were established from endogenous thyroid tumors developed by genetically engineered mice (*Tpo-Cre-ER*^{T2}*; BRAF*$^{Ca/+}$*; Trp53*$^{-/-}$, see below). Cell lines were authenticated through short tandem repeat profiling (STR) either by the MD Anderson Cytogenetic Core facility (human cell lines) or by IDEXX BioAnalytics (North Grafton, MA)(mouse cell lines). All lines were routinely tested for *Mycoplasma* by PCR. Cells were maintained in RPMI growth media supplemented with glutamine, pyruvate, penicillin/streptomycin, and 10% fetal bovine serum. All reagents were purchased from Thermo Scientific (Waltham, MA).

Long-term cultures for testing resistance

Separate dishes of MDA-T85 cells were cultured long-term for 32 passages (32 weeks/8 months) in the continuous presence of 0.03% DMSO (control) or 5 μM dabrafenib in 0.03% DMSO in RPMI media. Cell subpopulations were labeled MTA-T85.R0 (control) and MTA-T85.R2 to MTA-T85.R8 according to the number of months kept in long-term cultures. The overall passage number status of these subpopulations of cells following the long-term dabrafenib treatment was p40 from their original line derivation. Following the long-term dabrafenib treatment, the resistant cell subclones' genetic identity was confirmed with STR fingerprinting. IC_{50} for dabrafenib in these subclones was measured by culturing the cells at 0.0, 0.01, 0.1, 1.0, 5 and 10 μM of the drug in 0.1% v/v DMSO. Three biological replicates were

performed. A nontreated plate was fixed and nuclei stained with 4′,6-diamidino-2-phenylindole (DAPI) at the time of drug treatment (Day 0) to provide the number of cells present at the start of treatment as previously described (32). After 72 hours of incubation in the presence of drug or 0.03% v/v DMSO (negative control), plates were fixed with 0.4% paraformaldehyde and nuclei stained with DAPI using an integrated HydroSpeed plate washer (Tecan Life Sciences) and Multidrop Combi dispenser. Plates were imaged on an IN Cell Analyzer 6000 laser-based confocal imaging platform (General Electric Healthcare Bio-Sciences) and nuclei counted using the algorithms developed using the IN Cell Developer Toolbox software (version 1.6). Dabrafenib and trametinib resistance were confirmed by using real-time live cell imaging of T85-R0 and T85-R4 cell growth in an IncuCyte® S3 System (Sartorius, Bohemia, NY). Cells were plated in 96-well plates in triplicates and imaged for 72 hours in the presence of either dabrafenib or trametinib at the indicated concentrations.

DNA sequencing

Whole exome sequencing (WES) of DNA samples from MDA-T85 cells treated long-term with 5 μM dabrafenib as described above and collected at month 0 (R0), month 2 (R2), month 4 (R4) and month 8 (R8) was performed by the MD Anderson Cancer Center Advanced Technology Genomics Core (ATGC). For comparison, DNA samples were collected from MDA-T85 cells treated long-term with 0.03% DMSO and collected at month 0, month 2, month 4, and month 8 of treatment.

The BWA-MEM algorithm was used to align raw sequencing reads to the human reference genome (GRCh38). The resulting alignments were processed to generate sorted BAM files. Duplicate reads were marked using Picard MarkDuplicates. Base quality score recalibration

was performed using GATK BaseRecalibrator. Somatic single nucleotide variants (SNVs) and small insertions/deletions (indels) were called using GATK Mutect2. Dabrafenib-resistant and matched DMSO BAM files were analyzed jointly to identify new somatic mutations. Variant filtration was applied using GATK FilterMutectCalls to remove low-quality calls. Variants were annotated using Funcotator.

Copy number alterations were detected from the WES data using GATK ModelSegments. Segmented copy number data were then analyzed using GISTIC2.0 to identify significantly amplified and deleted regions across samples. GISTIC was run using a q-value threshold of 0.25 and a confidence level of 0.95 for identifying driver copy number events.

Mouse model and mouse cell lines

Mouse studies were approved by the University of Texas MD Anderson Cancer Center Institutional Animal Care and Use Committee (IACUC) and conducted in compliance with the NIH Guide for the Care and Use of Laboratory Animals and the IACUC-approved protocols. All mice were obtained from the Jackson Laboratory. An ATC transgenic mouse model was generated as described by McFadden et al (33). Briefly, a *Tpo-Cre-ER*^{T2}*; BRAF*$^{Ca/+}$*; Trp53*$^{fl/fl}$ transgenic strain was created. Upon administration of tamoxifen in 2 months old mice, the animals developed thyroid tumors after a latency time of 3-4 months, as expected. Tumor growth was followed using MRI, then tumors excised after animal euthanasia. For histopathology, tumor fragments were fixed in Bouin's fixative, dehydrated using increasing ethanol concentrations and xylene, and then embedded in paraffin. After deparaffinization and rehydration, 5 µm tissue sections were prepared and stained for hematoxylin and eosin. Histological analysis demonstrated an evident pattern of undifferentiated cells resembling human ATC, with small

clusters of PTC cells in one of seven tumors analyzed (Supplementary Figures 1A and 1B). Five cell lines were derived from 18 different ATC mice and characterized (for genotypes of some lines, see Supplementary Figure 1C). Only two cell lines, MCH2.2 and PPA-6, were used in this study. Genotypes before (mouse tails) and after *Cre* recombination (tumors and cell lines) were assessed with the appropriate primer pairs (https://jacks-lab.mit.edu/protocols). Mouse ATC cell lines were cultured in RPMI growth media supplemented with glutamine, pyruvate, penicillin/streptomycin, and 10% fetal bovine serum (all reagents from Thermo Fisher Scientific).

Analyses of publicly available datasets

Gene expression values of ETV5, p38, and MEF2A comparing human ATC cells to normal thyroid cells were obtained from publicly available databases (NCBI-GEO GSE65144 (34) and GSE33630 (35)). Data were extracted from 23 ATC samples and 57 normal thyroid samples. The probe expression matrices we downloaded had been preprocessed and standardized. Correlations between ETV5 expression, p38 expression, and expression of components of the MAPK14 pathway were obtained from The Cancer Genome Atlas (TCGA) using cBioPortal (1).

Gene downregulation with shRNA and validation/quantification

Lentivirus particles containing ETV5-shRNA or control shRNA (scrambled) were used to infect MDA-T85 cells (MISSION® shRNA, Sigma-Aldrich, St Louis, MO). Transfected cells were selected in media containing 2 µg/mL puromycin (Clontech/Takara Bio, Mountain View, CA). Expression of ETV5 and two known ETV5 targets (TWIST1, SNAI1, Supplementary

Table S2) were quantified by quantitative real-time PCR (qRT-PCR) to validate the downregulation of ETV5 expression.

Quantitative real-time PCR

Total RNA was isolated using the Zymed Laboratories kit (Thermo Fisher Scientific, Waltham, MA, USA). cDNA was produced with the SuperScript VILO master MIX (Thermo Fisher Scientific, Waltham, MA, USA). Quantitative real-time PCR (qRT-PCR) was performed using Taqman probes from Applied Biosystems (Thermo Fisher Scientific, Waltham, MA, USA) (Supplementary Table S2). All analyses were performed according to (31). In brief, the expression value of each gene was normalized to the expression of an internal control gene (GAPDH or ACTB, ΔCt), then compared to experimental controls using the ΔΔCt method (fold change). qRT-PCR was performed with three technical replicates per sample and experiment, along with a minimum of three independent experiments. p-values ≤ 0.05 were considered significant.

Western blot analysis and quantification

Cells were lysed in a buffer made of 50 mM HEPES, pH 7.5, 1% (vol/vol) Igepal-C630, 1 mM EDTA, 10 mM NaF, 1 mM sodium orthovanadate, 5% (vol/vol) glycerol, 50 mM NaCl, and 1 mM PMSF (36). Halt Protease Inhibitor Cocktail and Phosphatase Inhibitor Cocktail were added at standard concentrations. All reagents were purchased from Thermo Fisher Scientific, Waltham, MA. Lysates were boiled at 100°C for 5 minutes, briefly centrifuged, and the supernatant loaded onto 10 % polyacrylamide or 4% to 12% Stain-Free TGX gels (5-25 µg/lane) (Bio-Rad, Hercules, CA). After separation, proteins were transferred onto nitrocellulose

or PVDF membranes with a Trans-Blot Turbo Transfer System (Bio-Rad, Hercules, CA). Membranes were blocked with 5% BSA in Tris buffer saline with 0.1% Tween 20 (TBST) for 60 minutes, or EveryBlot Blocking Buffer (Bio-Rad, Hercules, CA) for 5 min. The blots were incubated with antibodies recognizing human ETV5, human p38, human phospho-p38, or additional components of the p38 signaling pathway (Supplementary Table S3). Anti-ACTB, Vinculin, or GAPDH were used as loading controls (Supplementary Table S3). Blots were incubated with primary antibodies at 4°C overnight. After washing with TBST, the membranes were incubated with the appropriate horseradish peroxidase-conjugated secondary antibodies (Supplementary Table S3) for 1 hour at room temperature. Blots were washed and incubated with chemiluminescence substrates (SuperSignal West Dura #34095 and SuperSignal™ West Femto #34095, Thermo Fisher Scientific, Waltham, MA) and visualized with a ChemiDoc MP Imager imaging system (Bio-Rad, Hercules, CA). Protein band intensities were quantified using ImageJ software (NIH) or Image Lab 6.1 (Bio-Rad).

High-throughput drug screening

High-throughput screens were performed by the Gulf Coast Consortia's (GCC) Combinatorial Drug Discovery Program at Texas A&M Health Science Center Institute of Bioscience and Technology. Cell lines were screened against dabrafenib (a $BRAF^{V600E}$ inhibitor), several p38 kinase inhibitors (ralimetinib, PD169316, SB203580), harmine (a putative TWIST1 inhibitor), venetoclax (a BCL2 inhibitor), a MMP9 inhibitor, xanthohumol (a prenylated chalconoid), and the cytotoxic agents anysomycin and doxorubicin (positive controls). The cell lines MDA-T68 (PTC, with a dominant follicular component) and Hth83 (ATC) were used as negative controls as they do not harbor any BRAF mutation. For screening assays, a total of 500

cells in 50 μL RPMI media were seeded in each well of black high binding uClear® 384-well polystyrene plates (Greiner Bio-One, Monroe, NC) using a Multidrop Combi liquid dispenser (Thermo Fisher Scientific, Waltham, MA). After seeding, the plates were held at room temperature for 45-60 min and placed into a humidified cell culture incubator with 5% CO_2 at 37°C. The cells were allowed to form a monolayer overnight, then 50 nL of drugs at different concentrations were transferred into each well using an Echo 550 acoustic dispensing platform (Labcyte/Beckman Coulter, Indianapolis, IN). The drugs were tested at a final concentration of 0.00, 0.01, 0.10, and 1.00 μM in 0.1% v/v DMSO. Two biological replicates were performed. A nontreated plate was fixed and nuclei stained with 4′,6-diamidino-2-phenylindole (DAPI) to provide the number of cells present at the start of drug treatment (Day 0) as previously described (32). After 72 hours of incubation in the presence of drug or 0.1% v/v DMSO (negative control), plates were fixed with 0.4% paraformaldehyde and nuclei stained with DAPI using an integrated HydroSpeed plate washer (Tecan Life Sciences) and Multidrop Combi dispenser. Plates were imaged on an IN Cell Analyzer 6000 laser-based confocal imaging platform (General Electric Healthcare Bio-Sciences) and nuclei counted using the algorithms developed using the IN Cell Developer Toolbox software (version 1.6) (32).

Statistical evaluation was performed on each plate throughout the course of the screening to assess the consistency of results as previously described (32). Metrics evaluated included the rate of growth of the negative controls, the coefficient of variance of the positive and negative controls, and assay robustness determined from the *z*-scores. Assay reproducibility and experimental drift were determined as previously reported (32). We used the normalized growth rate inhibition algorithm which quantifies the cellular response to drugs (37).

High-throughput screening combination of anchor and probes

We performed a high-throughput combination screen using an anchor-probe strategy on six cell lines (MDA-T85, MDA-T68, Hth83, SW1736, MCH2.2 and PPA-6). Dabrafenib, a $BRAF^{V600E}$ inhibitor, was chosen as the anchor drug due to its FDA-approved use in ATC patients (7). Dabrafenib was combined with seven inhibitor compounds that target pathways identified from public databases or array analyses (26). Those inhibitors were p38 inhibitors (ralimetinib, PD169316, SB203580), harmine (a putative TWIST1 inhibitor), venetoclax (a BCL2 inhibitor), and xanthohumol (a prenylated chalconoid), Eight concentrations of probe molecules were tested in pairwise combination with five concentrations of the anchor drug (100, 55, 30, 20, and 10 nmol/L). Drug interactions were categorized as synergistic, additive or antagonistic by comparing the experimentally observed dose response surface to a theoretical surface calculated from the independent single-agent activity using a Bliss synergy model as previously described (32). As a cutoff, we used the sum of all pairwise interactions to define antagonism (< -1) or synergy ($> +1$), respectively. Additional drug synergy metrics, including excess over the highest single agent, Loewe additivity, and zero interaction potency, were calculated using the SynergyFinder Plus R package. In addition to provide expanded metrics that quantify drug synergy, this package also uses a bootstrapping method to evaluate the statistical significance of the drug-drug interaction, thus providing a robust evaluation of drug-drug synergy.

Animal treatments

For a preliminary assessment, syngeneic mice (equal number of male and females) were subcutaneously (flank) injected with approximately 1×10^6 MCH2.2 mouse ATC cells. Tumor

growth was measured with a caliper. Treatments were initiated once the tumors achieved a volume of 100 mm^3, about 10 days after cell injection. The mice were randomly divided into treatment groups of five mice each: vehicle control (0.01% DMSO in phosphate buffered saline), dabrafenib ($BRAF^{V600E}$ inhibitor), ralimetinib (p38/MAPK14 inhibitor), PD169313 (p38/MAPK14 inhibitor), SB203580 (p38/MAPK14 inhibitor), harmine (TWIST1 inhibitor), and xanthohumol (NOTCH inhibitor). All drugs were prepared at a final concentration of 30 mg/kg in 0.01% DMSO and injected as single treatments. Tumor size was recorded for another 12 days, and all mice were euthanized at that point. A Kaplan-Meier survival graph with the different treatments was established.

For drug combination studies with mice bearing endogenous tumors, *TPO-Cre-ER*^{T2}*; BRAF*$^{Ca/+}$*; Trp53*$^{fl/fl}$ transgenic mice were treated with tamoxifen using standard procedures (Jackson Laboratory). After 3 months, tumor volumes were regularly measured using MRI until the end of treatments. Once thyroid tumors reached a volume of ~100 mm^3, mice (6 mice per treatment) were treated with dabrafenib (0, 6, 12, or 30 mg/kg), ralimetinib (0 or 30 mg/kg), or a combination of dabrafenib and ralimetinib (0/0, 6/30, 9/30, 12/30, or 30/30 mg/kg/day respectively). A combination of dabrafenib (6 mg/kg/day) and trametinib (0.6 mg/kg/day) was used as benchmark. Tumors were measured every 5 days for 21 days using MRI and recorded as percent change in tumor growth compared to tumor volume on day 0 of treatment.

Statistical analysis

Student *t*-tests or one-way ANOVA were used to compare two or more groups. For data with a nonparametric distribution, the Mann–Whitney–Wilcoxon test was used to compare two samples or groups. A *P* value less than 0.05 was considered statistically significant. All statistical tests were two-sided.

Data Availability

The data generated in this study are available within the article and its supplementary data files.

Results

Expression of the transcription factor ETV5 in ATC patient samples and cell lines

We previously demonstrated that the transcription factor ETV5 is expressed downstream of BRAF or RAS mutations in PTC patient samples and a PDTC cell line, KTC1 (26). In these cells, ETV5 enhanced growth and acted as a driver of TWIST1 gene expression, which is a well-known mediator of epithelial-to-mesenchymal transition (38). Our GEO databases analyses of ATC patient samples indicated that expression of *ETV5* mRNA and its target *TWIST1* are also significantly upregulated in ATC patient samples compared to normal thyroid tissues (Figure 1A-D). Further, as shown by western blotting, ETV5 protein was prominently expressed in several PTC and ATC cell lines (Figures 1E and 1F), particularly in the nucleus, as shown by its co-expression with nuclear lamin A (nuclear extracts). ETV5 expression was rapidly down-regulated by $BRAF^{V600E}$ inhibitors in short-term treatments (48 hours) and this effect was dose-dependent. However, dabrafenib was more efficient than vemurafenib in two mouse ATC cell lines (MCH2.2 and PPA6) and a human PDTC cell line (MDA-T85) (Figure 1G). Dabrafenib induced paradoxical ERK1/2 activation, particularly in the MDA-T85 cells, confirming previous findings (39). Further, ETV5 expression was significantly upregulated in a subclone of KTC1 PDTC cells (KTC1-VA7) that acquired a secondary $KRAS^{G12D}$ mutation upon long-term

treatment (5 months) with vemurafenib and became resistant to $BRAF^{V600E}$ inhibitors (38) (Figure 1H).

Resistance to dabrafenib in PDTC cells is associated with increased ETV5 and p38 activity

To confirm ETV5 upregulation at resistance, we next established another BRAF inhibitor resistant model, whereby MDA-T85 PDTC cells were cultured long-term (up to 8 months) with 5 µM dabrafenib. Cells were assessed every month (R0 to R8) for drug resistance (IC_{50}) and expression of ETV5 and ERK1/2 activity. Dabrafenib resistance was demonstrated by an increase in IC_{50} that reached > 50 µM at 3-4 months of culture (Figure 2A). Interestingly, these cells also became resistant to trametinib and continued growing compared to drug-sensitive cells despite the high drug concentrations (5-20 µM) (Figures 2B and 2C). We also observed a decrease of ETV5 protein expression during the first months of dabrafenib exposure, followed by a steady recovery over time (Figure 2D). As no specific pharmacological inhibitor of ETV5 is available, we performed in silico analysis to identify molecules that correlate with ETV5 expression in BRAF-mutated thyroid cancers. We first mined TCGA through cBioportal to analyze mRNA of 496 PTC samples (1). Results indicated that *ETV5* mRNA expression correlated strongly with *MAPK14* (also called *p38*) expression, a kinase often regulated by cellular stress, which also has oncogenic properties (40,41) (Figure 3A). We also observed that p38 expression and phosphorylation/activity follows ETV5 expression over time in dabrafenib-resistant cells (Figure 2D). In addition, expression of *MAP3K2*, a component of the p38MAPK cascade that leads to p38 activation, correlated with that of mutated *BRAF* (Figure 3B). Further, as shown in Figure 3C, we found *p38* mRNA significantly upregulated in ATC patient samples compared to normal thyroid tissues. MRNA expression of *MEF2A*, a target of the activated p38

protein, was also increased in ATC samples (Figure 3D). In addition, p38 protein and its activated/phosphorylated form, as well as ATF2/7, a known target of activated p38, were found in all PDTC and ATC cell lines tested (Supplementary Figure 2).

p38 expression and activity depend on ETV5 expression

To investigate whether ETV5 is responsible for p38 expression/activation, or, conversely, if p38 activity indirectly drives ETV5 expression, we employed shRNA to downregulate *ETV5* in MDA-T85 PDTC cells. This down-regulation was confirmed by assessing the expression levels of its targets, *TWIST1* and *SNAI1*, as depicted in Figure 3E. The observed decrease in both *TWIST1* and *SNAI1* mRNA expression validated the effective inhibition of *ETV5* and provided further support for the involvement of ETV5 in driving epithelial-to-mesenchymal transition (EMT) in these cells (26). Downregulation of *ETV5* expression by shRNA decreased p38 protein expression and significantly inhibited p38 phosphorylation/activity, as observed in Figures 3F and 3G. This observation suggests a functional interrelationship between these two molecules/pathways. Additionally, the reduced phosphorylation of MAPKAPK2 (or MK2), an immediate downstream target of p38 (41), further confirmed the alteration of p38 activity. Downregulation of ETV5 expression also caused a concomitant decrease in the expression and activity of MKK3/6 kinases. Because these kinases are known triggers of p38 activity (41), our data position ETV5 as a possible upstream regulator of the p38 pathway (Figure 3H). Therefore, through ETV5 upregulation, the MAPK pathway might activate the p38 pathway in thyroid cancer cells. We next assessed the sensitivity of several human and mouse PDTC and ATC cell lines to ralimetinib, a p38 inhibitor (Figure 3I). Our data indicate that IC_{50} for ralimetinib is 10-13 μM and that the drug equally affects BRAF mutated and BRAF wild-type cell lines.

High-throughput drug screening identifies synergism between dabrafenib and ralimetinib

Due to the significant occurrence of drug resistance in PDTC and ATC patients and possible cardiovascular adverse events linked to MEK inhibitors (42), it is imperative to explore alternative treatment options that can be combined with dabrafenib. Among these alternatives, we identified various pharmacological inhibitors of p38, including ralimetinib, which has been investigated in phase I trials involving patients with diverse solid tumors and lymphomas, often in conjunction with chemo- and radiotherapies (43-45). Thus, in this study, we investigated the effects of p38 inhibition in combination with dabrafenib in $BRAF^{V600E}$-mutated PDTC and ATC cells, and in animal models.

For each cell type, IC_{50} values were determined for each inhibitor (Supplementary Table S4). Dabrafenib IC_{50} values were high (>30 µM) for both BRAF wild-type cell lines (MDA-T68 and Hth83), as expected. The independent single-agent activities were used to calculate theoretical surfaces. Synergy Scores were obtained by comparing the experimentally observed dose response surface to the theoretical surface and calculated using the difference from Bliss (32,46)(Supplementary Table S5). Drug concentrations of ralimetinib and dabrafenib were categorized as synergistic (green), additive (black) or antagonistic (red) (Figure 4A-4D and Supplementary Table S5). Figures 4A'- 4D' show the corresponding synergy scores for each drug and cell line, with grouping into synergy (>1.00, green), additivity (-1.00 to +1.00, yellow), and antagonism (<-1.00, red). In MDA-T85 cells, which harbor a $BRAF^{V600E}$ and $HRAS^{Q61K}$ mutations, no inhibitor showed significant synergy in combination with dabrafenib (Figure 4A'). Only additivity was detected as well as some antagonistic effects of harmine (TWIST1 inhibitor) and PD169316 (p38 inhibitor). In MDA-T68 cells, which harbor solely $NRAS^{Q61K}$ as a driver

mutation and were used as negative controls, only xanthohumol, a flavonoid with potential NOTCH signaling inhibitory activity, led to significant inhibition. Furthermore, the ATC cell line Hth83, which is BRAF wild type but harbors a *HRAS*^{Q61R} and a *TP53*^{P152fs,P153fs} mutations, was also used as a negative control and exhibited no synergistic response by any statistical model. However, in SW1736, MCH2.2 and PPA-6 cells (Figure 4B-D and 4B'-D'), which all harbor a *BRAF*^{V600E} and a *TP53* nonsense mutation or deletion, p38 inhibitors significantly synergized with dabrafenib. The combination ralimetinib-dabrafenib exhibited the most consistent response. Because the identity of the ralimetinib target is controversial and could be the EGFR kinase rather than p38 (47), we tested the effect of ralimetinib on the activities/phosphorylation of p38, MK2 (downstream of p38), and EGFR in two cell lines (MTA-T85 and Hth83). In both cell lines, ralimetinib significantly inhibited MK2 phosphorylation, but did not significantly inhibit p38 nor EGFR activity (Supplementary Figure 3). Therefore, in PDTC and ATC cells, ralimetinib does inhibit the p38/MAPK14 pathway and decreases cell proliferation (Figure 3I and Supplementary Table S4) but uses a mechanism that differs from its effects in other cancer cell types (47).

Ralimetinib synergizes with dabrafenib in dabrafenib-resistant cells

We next assessed how dabrafenib resistance affected the response to pharmacological inhibitors and whether ralimetinib could re-sensitize resistant tumor cells in combination treatments. In MDA-T85 cells, synergy between dabrafenib and ralimetinib appeared at month 4 (R4) of dabrafenib resistance and lasted to month 8 (R8) (Figure 5), indicating that inhibition of the p38 pathway can resensitize the cancer cells to dabrafenib, and that p38 might be involved in drug resistance. Our data also indicate that the *TP53* mutation status of the tumor cells

(truncation versus gain-of-function) is relevant because *BRAF*^{V600E}*/TP53* truncated cells were more sensitive to the combination treatment (dabrafenib 0.1-50 nM, Figure 4) than *BRAF*^{V600E}*/TP53* gain-of-function cells (dabrafenib ≥15 µM, Figure 5).

Resistance to dabrafenib in MDA-T85 cells parallels a *TP53*^{R248W} driver mutation

Whole exome sequencing of MDA-T85 cells exposed long-term to dabrafenib (R0 to R8 samples) revealed a variety of mutations compared to cells exposed to DMSO only. Overall, the number of additional novel mutations increased with the duration of drug exposure (Figure 6A). Most mutations were passenger mutations; however, one documented driver mutation, *TP53*^{R248W}**,** appeared between month 4 and 8 of dabrafenib exposure (Figure 6A and Supplementary Table S6). A splice site mutation also occurred in this gene that was deemed not pathogenic. Accumulation of mutations over time indicated an increase of genomic instability possibly driven by dabrafenib. Most mutations were missense mutations (55%), followed by nonsense mutations (7%) and frame shifts/deletions (5%). Most single-nucleotide variants (SNVs) were C>T followed by T>C and C>A and the median SNVs per sample was 15. Finally, GISTIK copy number analysis revealed significant changes mostly at month 8 of dabrafenib exposure (Figure 6B and Supplementary Table S7), with amplifications of chromosome 1 (p+q) and substantial deletions in chromosome 8 (p+q), 15q, and 18 (p+q). Chromosome 1 amplification, particularly of the 1q arm, is a recurring event in thyroid cancers and may be associated with more aggressive or advanced disease states, possibly through amplification of *NRAS* and *SRC* (48). None of the observed chromosomal deletions affected genes known to drive aggressive thyroid cancers, including at drug resistance (*TP53, PTEN, PIK3CA, ATM, ATR, NF1, NF2, BRCA1/2*).

Ralimetinib combined with dabrafenib shows some synergy in ATC mouse models

To assess the effect of p38/MAPK inhibitors in ATC mouse models, we first tested these drugs by xenografting MCH2.2 mouse tumor cells in syngeneic C57Bl/6 mice (flank injections). Mice were euthanized when tumors reached a volume of 100% of initial volume. Ralimetinib and dabrafenib yielded similar responses (~50% of mice survived beyond day 15 of treatment) (Figure 6C) both at the dose of 30 mg/kg/day. Other p38 inhibitors (PD169313 and SB203580) had only transient effects and these mice were euthanized at day 12 of treatment (median survival = 12 days), as were the control animals (median survival = 8 days).

We then assessed different doses of dabrafenib in combination with trametinib (dabrafenib 0, 6, 12 and 30 mg/kg/day; trametinib 0 and 0.6 mg/kg/day) in *Braf*$^{+/CA}$; *Trp53*$^{del/del}$ ATC mice. Tumor volumes were assessed using MRI. Data indicated that, in these mice, dabrafenib (6 or 12 mg/kg/day) in combination with trametinib (0.6 mg/kg/day) significantly reduced tumor growth compared to the control treatment (DMSO only). Therefore, to assess synergy, the lower dabrafenib dose (6 mg/mg/kg) was tested alone and in combination with ralimetinib or trametinib. During the first 9 days of treatment, the dabrafenib-ralimetinib combination was as effective as the dabrafenib-trametinib combination but this effect did not persist as smaller tumor volume reductions were detected on day 15 and beyond (Figures 6D and 6E).

Discussion

In this study, we identified the p38/MAPK14 pathway as a downstream target of ETV5 in PDTC and ATC preclinical models. Inhibiting p38 signaling with pharmacological inhibitors reduced tumor cell growth and showed drug synergy with dabrafenib. Our data also indicate that the mutational status of *TP53* might affect the response to p38 inhibitors, particularly in dabrafenib-resistant cells.

The ETS family of transcription factors contains 28 homologs that can be categorized into 12 subfamilies (including ETS and PEA3) based on their sequence similarity and the positioning of the ETS domain (49,50). These transcription factors play crucial roles in various biological processes, including tumor progression (50). As shown in the present study, ETV5 was also expressed in multiple aggressive thyroid cancer cell lines (PDTC and ATC). Its expression was associated with activation of the MAPK pathway and was downregulated by dabrafenib, corroborating our previous data (26). Further, it was re-expressed at drug resistance, making it a potential marker for tumor progression. Because there is no drug effectively inhibiting ETV5 nor any PEA3 transcription factors, we focused on inhibiting one of its putative downstream targets, p38, also re-expressed at resistance.

p38 is a key player in the cellular response to stress and inflammation. It is essential for maintaining cellular homeostasis and mediating various signaling pathways, including p53. Dysregulation of p38 has been linked to several diseases, including inflammatory disorders, neurodegenerative diseases, and cancer progression (41,51). In our study, ralimetinib was the most effective of the p38 inhibitors tested, but there is recent controversy regarding the identity of its target (47). As demonstrated here, ralimetinib effectively downregulated the p38 pathway by specifically inhibiting the kinase activity of MK2, a direct downstream target of p38, but not

EGFR kinase activity. The observed synergy between dabrafenib and ralimetinib *in vitro*, and to some extent *in vivo*, supports the need for further preclinical investigations using p38 inhibitors with better specificity and efficiency.

Acquired, or secondary, resistance often develops after an initial period of response to kinase inhibitors, including combination therapies such as dabrafenib and trametinib. The mechanisms of drug resistance vary extensively among individuals and tumor types, and identification of these mechanisms should improve the clinical efficacy of treatments. Known mechanisms of resistance include target alteration, which reduces drug binding or increases kinase activity (52,53); novel gene driver mutations (16,23,31); bypass signaling that often activates the PI3K/AKT pathway (16,54-57); and growth factor receptors' amplification (19,31,58). Some of these resistance mechanisms have been observed using cell lines derived from melanoma, hepatocarcinoma or colon cancer in addition to patient samples. In this study, we used a BRAF inhibitor resistance model of aggressive thyroid cancer cells. Resistance to dabrafenib appeared between months 3 and 4 of drug exposure and was accompanied by resistance to trametinib as well. These features are similar to clinical observations (40) and our previous data obtained with another PDTC cell line (16). Absent additional genomic mutations in mediators of the MAPK or PI3K-AKT pathway, the cause of this concomitant resistance to trametinib might be the epigenetic upregulation of receptors such as EGFR1 (ERBB1) and ERBB3 (19), known for activating both the PI3K-AKT and MAPK pathways (59). This would also explain the rebound of ETV5 and concomitant p38 upregulation at resistance.

In BRAF-mutated solid tumors, common causes of resistance to dabrafenib and trametinib include *KRAS* or *NRAS* mutations (60). It is unknown whether selective pressure favors the development of pre-existing mutated subclones or whether BRAF inhibition itself

induces genomic instability over time. In the present study, confirming previous data (16), the secondary driver mutation was not detectable by WES at the start of treatment nor in parental cells. *TP53*^{R248W} is a hotspot gain-of-function mutation that occurs in the DNA-binding domain of the p53 protein. This mutation is one of the most commonly observed in cancers, particularly in those arising in the breast and head and neck regions where it is more potent in driving tumorigenesis and metastasis compared to other *TP53* mutations (61,62). As with other mutant p53 proteins, mutant p53^{R248W} undergoes strong Hsp90-mediated stabilization, leading to the accumulation of high protein levels in the nucleus and cytoplasm (63). Gain-of-function mutant p53 proteins interact with and significantly impact various signaling pathways, including the STAT3 and p38 pathways (64,65). In the present study, ralimetinib and its synergistic activity with dabrafenib were more efficient when p53 protein expression was deleted rather than overexpressed by a gain-of-function *TP53*^{R248W} secondary mutation. The indirect enhancement of MKK3/6 phosphorylation by both ETV5 and gain-of-function p53 could potentially shift p38 function toward a more aggressive oncogenic role (64,66,67), but further investigations are needed to understand this crosstalk in the context of PDTC/ATC. Also, a transcriptomic assessment of clonal evolution over time will help elucidate evolutionary patterns and shifts in gene expression associated with dabrafenib resistance.

In summary, ETV5, p38, and p53 play interconnected and critical roles in the regulation of PDTC/ATC cell behavior. ETV5, often associated with enhanced proliferation, migration, and metastasis in cancer, is tightly linked to signaling pathways such as p38/MAPK, which can exhibit dual roles (apoptosis or tumorigenesis) depending on the cellular context. The interaction between p38 and p53 mutation status adds further complexity. Dysregulation of this network can shift the balance between tumor suppression and growth, highlighting their combined importance

in cancer biology. We found that, in these cells, ralimetinib inhibited the p38 pathway by targeting MK2 activity, and significantly synergized with dabrafenib *in vitro* in presence of *TP53* mutations. Ralimetinib also synergized with dabrafenib during the initial days of ATC mice treatments. Despite the lack of sustained *in vivo* effects, our work has highlighted a novel resistance pathway and positioned ETV5 and p38 as key markers of tumor progression. Targeting the intricate crosstalk between these factors using improved p38, HSP90, or STAT3 inhibitors (68-70), possibly combined with immunotherapy, offers a promising avenue for developing more effective therapeutic strategies for these tumors.

Acknowledgements

This work was supported by the Anaplastic Thyroid Cancer Multidisciplinary Research Funds (JHH, RBY, YCH, AD, SYL, MCH); a University of Texas MD Anderson Cancer Center IRG Seed Grant (MCH); and DOD #HT9425-23-1-0675 (MCH). We also thank the Institute for Biotechnology (IBT) High Throughput Research and Screening Center at Houston (CPRIT grant number RP200668) and acknowledge the NIH/NCI for supporting the MD Anderson Cancer Center Core Facilities (NCI P30CA016672). Editorial support was provided by Bryan Tutt, Senior Scientific Editor, Research Medical Library at MD Anderson Cancer Center.

References

1. Cancer_Genome_Atlas_Research_Network. Integrated Genomic Characterization of Papillary Thyroid Carcinoma. Cell **2014**;159:676-90 doi https://doi.org/10.1016/j.cell.2014.09.050.
2. Kunstman JW, Juhlin CC, Goh G, Brown TC, Stenman A, Healy JM, *et al.* Characterization of the mutational landscape of anaplastic thyroid cancer via whole-exome sequencing. Hum Mol Genet **2015**;24(8):2318-29 doi 10.1093/hmg/ddu749.
3. Landa I, Ibrahimpasic T, Boucai L, Sinha R, Knauf JA, Shah RH, *et al.* Genomic and transcriptomic hallmarks of poorly differentiated and anaplastic thyroid cancers. J Clin Invest **2016**;126(3):1052-66 doi 10.1172/JCI85271.
4. Liu X, Bishop J, Shan Y, Pai S, Liu D, Murugan AK, *et al.* Highly prevalent TERT promoter mutations in aggressive thyroid cancers. Endocr Relat Cancer **2013**;20(4):603-10 doi 10.1530/ERC-13-0210.
5. Zeng PYF, Prokopec SD, Lai SY, Pinto N, Chan-Seng-Yue MA, Clifton-Bligh R, *et al.* The genomic and evolutionary landscapes of anaplastic thyroid carcinoma. Cell Rep **2024**;43(3):113826 doi 10.1016/j.celrep.2024.113826.
6. de la Fouchardiere C, Decaussin-Petrucci M, Berthiller J, Descotes F, Lopez J, Lifante JC, *et al.* Predictive factors of outcome in poorly differentiated thyroid carcinomas. European journal of cancer **2018**;92:40-7 doi 10.1016/j.ejca.2017.12.027.
7. Maniakas A, Dadu R, Busaidy NL, Wang JR, Ferrarotto R, Lu C, *et al.* Evaluation of Overall Survival in Patients With Anaplastic Thyroid Carcinoma, 2000-2019. JAMA Oncol **2020**;6(9):1397-404 doi 10.1001/jamaoncol.2020.3362.
8. Qin Y, Wang JR, Wang Y, Iyer P, Cote GJ, Busaidy NL, *et al.* Clinical Utility of Circulating Cell-Free DNA Mutations in Anaplastic Thyroid Carcinoma. Thyroid **2021**;31(8):1235-43 doi 10.1089/thy.2020.0296.
9. Davies H, Bignell GR, Cox C, Stephens P, Edkins S, Clegg S, *et al.* Mutations of the BRAF gene in human cancer. Nature **2002**;417(6892):949-54 doi 10.1038/nature00766.
10. Xing M, Liu R, Liu X, Murugan AK, Zhu G, Zeiger MA, *et al.* BRAF V600E and TERT promoter mutations cooperatively identify the most aggressive papillary thyroid cancer with highest recurrence. J Clin Oncol **2014**;32(25):2718-26 doi 10.1200/JCO.2014.55.5094.
11. Liu R, Zhang T, Zhu G, Xing M. Regulation of mutant TERT by BRAF V600E/MAP kinase pathway through FOS/GABP in human cancer. Nat Commun **2018**;9(1):579 doi 10.1038/s41467-018-03033-1.
12. Subbiah V, Kreitman RJ, Wainberg ZA, Cho JY, Schellens JHM, Soria JC, *et al.* Dabrafenib and Trametinib Treatment in Patients With Locally Advanced or Metastatic BRAF V600-Mutant Anaplastic Thyroid Cancer. J Clin Oncol **2018**;36(1):7-13 doi 10.1200/JCO.2017.73.6785.
13. Wang JR, Zafereo ME, Dadu R, Ferrarotto R, Busaidy NL, Lu C, *et al.* Complete Surgical Resection Following Neoadjuvant Dabrafenib Plus Trametinib in BRAF(V600E)-Mutated Anaplastic Thyroid Carcinoma. Thyroid **2019**;29(8):1036-43 doi 10.1089/thy.2019.0133.
14. Hamidi S, Iyer PC, Dadu R, Gule-Monroe MK, Maniakas A, Zafereo ME, *et al.* Checkpoint Inhibition in Addition to Dabrafenib/Trametinib for BRAF(V600E)-Mutated Anaplastic Thyroid Carcinoma. Thyroid **2024**;34(3):336-46 doi 10.1089/thy.2023.0573.

15. Cabanillas ME, Dadu R, Ferrarotto R, Gule-Monroe M, Liu S, Fellman B, *et al.* Anti-Programmed Death Ligand 1 Plus Targeted Therapy in Anaplastic Thyroid Carcinoma: A Nonrandomized Clinical Trial. JAMA Oncol **2024**;10(12):1672-80 doi 10.1001/jamaoncol.2024.4729.
16. Danysh BP, Rieger EY, Sinha DK, Evers CV, Cote GJ, Cabanillas ME, *et al.* Long-term vemurafenib treatment drives inhibitor resistance through a spontaneous KRAS G12D mutation in a BRAF V600E papillary thyroid carcinoma model. Oncotarget **2016**;7(21):30907-23 doi 10.18632/oncotarget.9023.
17. Baitei EY, Zou M, Al-Mohanna F, Collison K, Alzahrani AS, Farid NR, *et al.* Aberrant BRAF splicing as an alternative mechanism for oncogenic B-Raf activation in thyroid carcinoma. The Journal of pathology **2009**;217(5):707-15 doi 10.1002/path.2496.
18. Poulikakos PI, Persaud Y, Janakiraman M, Kong X, Ng C, Moriceau G, *et al.* RAF inhibitor resistance is mediated by dimerization of aberrantly spliced BRAF(V600E). Nature **2011**;480(7377):387-90 doi 10.1038/nature10662.
19. Montero-Conde C, Ruiz-Llorente S, Dominguez JM, Knauf JA, Viale A, Sherman EJ, *et al.* Relief of feedback inhibition of HER3 transcription by RAF and MEK inhibitors attenuates their antitumor effects in BRAF-mutant thyroid carcinomas. Cancer Discov **2013**;3(5):520-33 doi 10.1158/2159-8290.CD-12-0531.
20. Yadav V, Zhang X, Liu J, Estrem S, Li S, Gong XQ, *et al.* Reactivation of mitogen-activated protein kinase (MAPK) pathway by FGF receptor 3 (FGFR3)/Ras mediates resistance to vemurafenib in human B-RAF V600E mutant melanoma. J Biol Chem **2012**;287(33):28087-98 doi 10.1074/jbc.M112.377218.
21. Duquette M, Sadow PM, Husain A, Sims JN, Antonello ZA, Fischer AH, *et al.* Metastasis-associated MCL1 and P16 copy number alterations dictate resistance to vemurafenib in a BRAFV600E patient-derived papillary thyroid carcinoma preclinical model. Oncotarget **2015**;6(40):42445-67 doi 10.18632/oncotarget.6442.
22. Antonello ZA, Hsu N, Bhasin M, Roti G, Joshi M, Van Hummelen P, *et al.* Vemurafenib-resistance via de novo RBM genes mutations and chromosome 5 aberrations is overcome by combined therapy with palbociclib in thyroid carcinoma with BRAF(V600E). Oncotarget **2017**;8(49):84743-60 doi 10.18632/oncotarget.21262.
23. Cabanillas ME, Dadu R, Iyer P, Wanland KB, Busaidy NL, Ying A, *et al.* Acquired Secondary RAS Mutation in BRAF(V600E)-Mutated Thyroid Cancer Patients Treated with BRAF Inhibitors. Thyroid **2020**;30(9):1288-96 doi 10.1089/thy.2019.0514.
24. Hofmann MC, Kunnimalaiyaan M, Wang JR, Busaidy NL, Sherman SI, Lai S, *et al.* Molecular mechanisms of resistance to kinase inhibitors in thyroid cancers. Endocr Relat Cancer **2022** doi 10.1530/ERC-22-0129.
25. Lee M, Untch BR, Xu B, Ghossein R, Han C, Kuo F, *et al.* Genomic and Transcriptomic Correlates of Thyroid Carcinoma Evolution after BRAF Inhibitor Therapy. Mol Cancer Res **2022**;20(1):45-55 doi 10.1158/1541-7786.MCR-21-0442.
26. Puli OR, Danysh BP, McBeath E, Sinha DK, Hoang NM, Powell RT, *et al.* The Transcription Factor ETV5 Mediates BRAFV600E-Induced Proliferation and TWIST1 Expression in Papillary Thyroid Cancer Cells. Neoplasia **2018**;20(11):1121-34 doi 10.1016/j.neo.2018.09.003.
27. Henderson YC, Ahn SH, Ryu J, Chen Y, Williams MD, El-Naggar AK, *et al.* Development and characterization of six new human papillary thyroid carcinoma cell

lines. The Journal of clinical endocrinology and metabolism **2015**;100(2):E243-52 doi 10.1210/jc.2014-2624.
28. Kurebayashi J, Tanaka K, Otsuki T, Moriya T, Kunisue H, Uno M, *et al.* All-trans-retinoic acid modulates expression levels of thyroglobulin and cytokines in a new human poorly differentiated papillary thyroid carcinoma cell line, KTC-1. The Journal of clinical endocrinology and metabolism **2000**;85(8):2889-96 doi 10.1210/jcem.85.8.6732.
29. Landa I, Pozdeyev N, Korch C, Marlow LA, Smallridge RC, Copland JA, *et al.* Comprehensive Genetic Characterization of Human Thyroid Cancer Cell Lines: A Validated Panel for Preclinical Studies. Clin Cancer Res **2019**;25(10):3141-51 doi 10.1158/1078-0432.CCR-18-2953.
30. Dahlman T, Lammerts E, Wik M, Bergstrom D, Grimelius L, Westermark K, *et al.* Fibrosis in undifferentiated (anaplastic) thyroid carcinomas: evidence for a dual action of tumour cells in collagen type I synthesis. The Journal of pathology **2000**;191(4):376-86 doi 10.1002/1096-9896(2000)9999:9999<::AID-PATH643>3.0.CO;2-W.
31. Bagheri-Yarmand R, Busaidy NL, McBeath E, Danysh BP, Evans KW, Moss TJ, *et al.* RAC1 Alterations Induce Acquired Dabrafenib Resistance in Association with Anaplastic Transformation in a Papillary Thyroid Cancer Patient. Cancers (Basel) **2021**;13(19) doi 10.3390/cancers13194950.
32. Handley KF, Rodriguez-Aguayo C, Ma S, Stur E, Joseph R, Bayraktar E, *et al.* Rational Combination of CRM1 Inhibitor Selinexor and Olaparib Shows Synergy in Ovarian Cancer Cell Lines and Mouse Models. Mol Cancer Ther **2021**;20(12):2352-61 doi 10.1158/1535-7163.MCT-21-0370.
33. McFadden DG, Vernon A, Santiago PM, Martinez-McFaline R, Bhutkar A, Crowley DM, *et al.* p53 constrains progression to anaplastic thyroid carcinoma in a Braf-mutant mouse model of papillary thyroid cancer. Proc Natl Acad Sci U S A **2014**;111(16):E1600-9 doi 10.1073/pnas.1404357111.
34. von Roemeling CA, Marlow LA, Pinkerton AB, Crist A, Miller J, Tun HW, *et al.* Aberrant lipid metabolism in anaplastic thyroid carcinoma reveals stearoyl CoA desaturase 1 as a novel therapeutic target. The Journal of clinical endocrinology and metabolism **2015**;100(5):E697-709 doi 10.1210/jc.2014-2764.
35. Tomas G, Tarabichi M, Gacquer D, Hebrant A, Dom G, Dumont JE, *et al.* A general method to derive robust organ-specific gene expression-based differentiation indices: application to thyroid cancer diagnostic. Oncogene **2012**;31(41):4490-8 doi 10.1038/onc.2011.626.
36. Houl JH, Ye Z, Brosey CA, Balapiti-Modarage LPF, Namjoshi S, Bacolla A, *et al.* Selective small molecule PARG inhibitor causes replication fork stalling and cancer cell death. Nat Commun **2019**;10(1):5654 doi 10.1038/s41467-019-13508-4.
37. Hafner M, Niepel M, Chung M, Sorger PK. Growth rate inhibition metrics correct for confounders in measuring sensitivity to cancer drugs. Nat Methods **2016**;13(6):521-7 doi 10.1038/nmeth.3853.
38. Zheng Y, Dai M, Dong Y, Yu H, Liu T, Feng X, *et al.* ZEB2/TWIST1/PRMT5/NuRD Multicomplex Contributes to the Epigenetic Regulation of EMT and Metastasis in Colorectal Carcinoma. Cancers (Basel) **2022**;14(14) doi 10.3390/cancers14143426.
39. Adelmann CH, Ching G, Du L, Saporito RC, Bansal V, Pence LJ, *et al.* Comparative profiles of BRAF inhibitors: the paradox index as a predictor of clinical toxicity. Oncotarget **2016**;7(21):30453-60 doi 10.18632/oncotarget.8351.

40. Corre I, Paris F, Huot J. The p38 pathway, a major pleiotropic cascade that transduces stress and metastatic signals in endothelial cells. Oncotarget **2017**;8(33):55684-714 doi 10.18632/oncotarget.18264.
41. García-Hernández L, García-Ortega MB, Ruiz-Alcalá G, Carrillo E, Marchal JA, Garcia MA. The p38 MAPK Components and Modulators as Biomarkers and Molecular Targets in Cancer. Int J Mol Sci **2022**;23(1):370-.
42. Mincu RI, Mahabadi AA, Michel L, Mrotzek SM, Schadendorf D, Rassaf T, *et al.* Cardiovascular Adverse Events Associated With BRAF and MEK Inhibitors: A Systematic Review and Meta-analysis. JAMA Netw Open **2019**;2(8):e198890 doi 10.1001/jamanetworkopen.2019.8890.
43. Patnaik A, Haluska P, Tolcher AW, Erlichman C, Papadopoulos KP, Lensing JL, *et al.* A First-in-Human Phase I Study of the Oral p38 MAPK Inhibitor, Ralimetinib (LY2228820 Dimesylate), in Patients with Advanced Cancer. Clin Cancer Res **2016**;22(5):1095-102 doi 10.1158/1078-0432.CCR-15-1718.
44. Vergote I, Heitz F, Buderath P, Powell M, Sehouli J, Lee CM, *et al.* A randomized, double-blind, placebo-controlled phase 1b/2 study of ralimetinib, a p38 MAPK inhibitor, plus gemcitabine and carboplatin versus gemcitabine and carboplatin for women with recurrent platinum-sensitive ovarian cancer. Gynecol Oncol **2020**;156(1):23-31 doi 10.1016/j.ygyno.2019.11.006.
45. Hideshima T, Podar K, Chauhan D, Ishitsuka K, Mitsiades C, Tai YT, *et al.* p38 MAPK inhibition enhances PS-341 (bortezomib)-induced cytotoxicity against multiple myeloma cells. Oncogene **2004**;23(54):8766-76 doi 10.1038/sj.onc.1208118.
46. Zhao W, Sachsenmeier K, Zhang L, Sult E, Hollingsworth RE, Yang H. A New Bliss Independence Model to Analyze Drug Combination Data. J Biomol Screen **2014**;19(5):817-21 doi 10.1177/1087057114521867.
47. Bhattacharjee D, Bakar J, Chitnis SP, Sausville EL, Ashtekar KD, Mendelson BE, *et al.* Inhibition of a lower potency target drives the anticancer activity of a clinical p38 inhibitor. Cell Chem Biol **2023**;30(10):1211-22 e5 doi 10.1016/j.chembiol.2023.09.013.
48. Ibrahimpasic T, Xu B, Landa I, Dogan S, Middha S, Seshan V, *et al.* Genomic Alterations in Fatal Forms of Non-Anaplastic Thyroid Cancer: Identification of MED12 and RBM10 as Novel Thyroid Cancer Genes Associated with Tumor Virulence. Clin Cancer Res **2017**;23(19):5970-80 doi 10.1158/1078-0432.CCR-17-1183.
49. Sizemore GM, Pitarresi JR, Balakrishnan S, Ostrowski MC. The ETS family of oncogenic transcription factors in solid tumours. Nat Rev Cancer **2017**;17(6):337-51 doi 10.1038/nrc.2017.20.
50. Feng FY, Brenner JC, Hussain M, Chinnaiyan AM. Molecular pathways: targeting ETS gene fusions in cancer. Clin Cancer Res **2014**;20(17):4442-8 doi 10.1158/1078-0432.CCR-13-0275.
51. Roy S, Roy S, Kar M, Padhi S, Saha A, Anuja K, *et al.* Role of p38 MAPK in disease relapse and therapeutic resistance by maintenance of cancer stem cells in head and neck squamous cell carcinoma. J Oral Pathol Med **2018**;47(5):492-501 doi 10.1111/jop.12707.
52. Jiang L, Li L, Liu Y, Lu L, Zhan M, Yuan S, *et al.* Drug resistance mechanism of kinase inhibitors in the treatment of hepatocellular carcinoma. Front Pharmacol **2023**;14:1097277 doi 10.3389/fphar.2023.1097277.

53. Zhong J, Yan W, Wang C, Liu W, Lin X, Zou Z, *et al.* BRAF Inhibitor Resistance in Melanoma: Mechanisms and Alternative Therapeutic Strategies. Curr Treat Options Oncol **2022**;23(11):1503-21 doi 10.1007/s11864-022-01006-7.
54. Atefi M, von Euw E, Attar N, Ng C, Chu C, Guo D, *et al.* Reversing melanoma cross-resistance to BRAF and MEK inhibitors by co-targeting the AKT/mTOR pathway. PloS one **2011**;6(12):e28973 doi 10.1371/journal.pone.0028973.
55. Han P, Li H, Jiang X, Zhai B, Tan G, Zhao D, *et al.* Dual inhibition of Akt and c-Met as a second-line therapy following acquired resistance to sorafenib in hepatocellular carcinoma cells. Mol Oncol **2017**;11(3):320-34 doi 10.1002/1878-0261.12039.
56. Janku F, Yap TA, Meric-Bernstam F. Targeting the PI3K pathway in cancer: are we making headway? Nat Rev Clin Oncol **2018**;15(5):273-91 doi 10.1038/nrclinonc.2018.28.
57. Chen KF, Chen HL, Tai WT, Feng WC, Hsu CH, Chen PJ, *et al.* Activation of phosphatidylinositol 3-kinase/Akt signaling pathway mediates acquired resistance to sorafenib in hepatocellular carcinoma cells. J Pharmacol Exp Ther **2011**;337(1):155-61 doi 10.1124/jpet.110.175786.
58. Arao T, Ueshima K, Matsumoto K, Nagai T, Kimura H, Hagiwara S, *et al.* FGF3/FGF4 amplification and multiple lung metastases in responders to sorafenib in hepatocellular carcinoma. Hepatology **2013**;57(4):1407-15 doi 10.1002/hep.25956.
59. Black LE, Longo JF, Carroll SL. Mechanisms of Receptor Tyrosine-Protein Kinase ErbB-3 (ERBB3) Action in Human Neoplasia. Am J Pathol **2019**;189(10):1898-912 doi 10.1016/j.ajpath.2019.06.008.
60. Johnson DB, Menzies AM, Zimmer L, Eroglu Z, Ye F, Zhao S, *et al.* Acquired BRAF inhibitor resistance: A multicenter meta-analysis of the spectrum and frequencies, clinical behaviour, and phenotypic associations of resistance mechanisms. European journal of cancer **2015**;51(18):2792-9 doi 10.1016/j.ejca.2015.08.022.
61. Zhang Y, Xiong S, Liu B, Pant V, Celii F, Chau G, *et al.* Somatic Trp53 mutations differentially drive breast cancer and evolution of metastases. Nat Commun **2018**;9(1):3953 doi 10.1038/s41467-018-06146-9.
62. Li M, Sun D, Song N, Chen X, Zhang X, Zheng W, *et al.* Mutant p53 in head and neck squamous cell carcinoma: Molecular mechanism of gain□of□function and targeting therapy (Review). Oncol Rep **2023**;50(3) doi 10.3892/or.2023.8599.
63. Wawrzynow B, Zylicz A, Zylicz M. Chaperoning the guardian of the genome. The two-faced role of molecular chaperones in p53 tumor suppressor action. Biochim Biophys Acta Rev Cancer **2018**;1869(2):161-74 doi 10.1016/j.bbcan.2017.12.004.
64. Stramucci L, Pranteda A, Bossi G. Insights of Crosstalk between p53 Protein and the MKK3/MKK6/p38 MAPK Signaling Pathway in Cancer. Cancers (Basel) **2018**;10(5) doi 10.3390/cancers10050131.
65. Stramucci L, Pranteda A, Stravato A, Amoreo CA, Pennetti A, Diodoro MG, *et al.* MKK3 sustains cell proliferation and survival through p38DELTA MAPK activation in colorectal cancer. Cell Death Dis **2019**;10(11):842 doi 10.1038/s41419-019-2083-2.
66. Stramucci L, Bossi G. Approaching the challenges of MKK3/p38delta MAPK targeting for therapeutic purpose in colorectal cancer. J Exp Clin Cancer Res **2019**;38(1):504 doi 10.1186/s13046-019-1513-4.
67. Piastra V, Pranteda A, Bossi G. Dissection of the MKK3 Functions in Human Cancer: A Double-Edged Sword? Cancers (Basel) **2022**;14(3) doi 10.3390/cancers14030483.

68. Klemke L, Fehlau CF, Winkler N, Toboll F, Singh SK, Moll UM, *et al.* The Gain-of-Function p53 R248W Mutant Promotes Migration by STAT3 Deregulation in Human Pancreatic Cancer Cells. Front Oncol **2021**;11:642603 doi 10.3389/fonc.2021.642603.
69. Carter BZ, Mak PY, Muftuoglu M, Tao W, Ke B, Pei J, *et al.* Epichaperome inhibition targets TP53-mutant AML and AML stem/progenitor cells. Blood **2023**;142(12):1056-70 doi 10.1182/blood.2022019047.
70. Kong R, Bharadwaj U, Eckols TK, Kolosov M, Wu H, Cruz-Pavlovich FJS, *et al.* Novel STAT3 small-molecule inhibitors identified by structure-based virtual ligand screening incorporating SH2 domain flexibility. Pharmacol Res **2021**;169:105637 doi 10.1016/j.phrs.2021.105637.

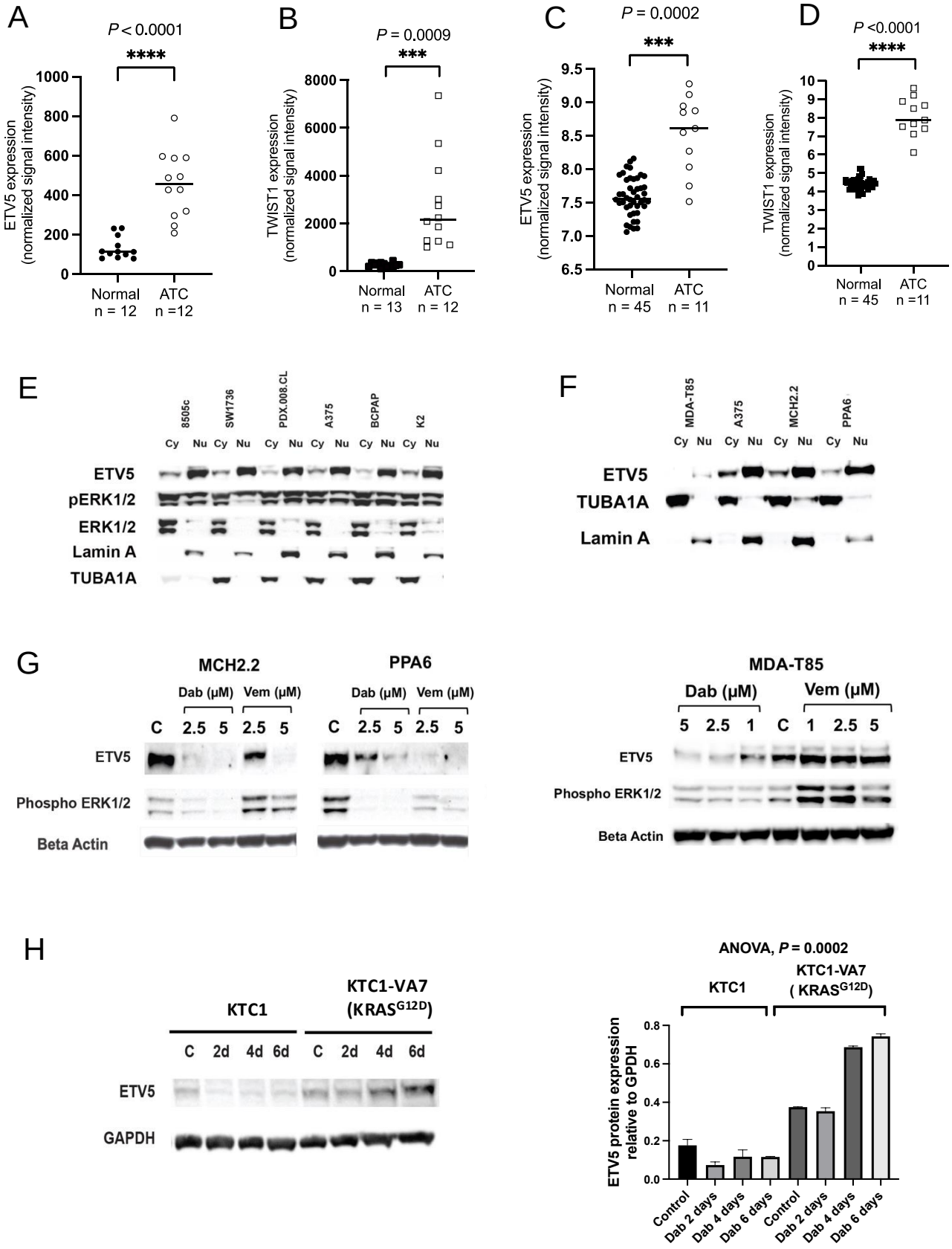
A
P < 0.0001
****
ETV5 expression (normalized signal intensity)
Normal n = 12
ATC n =12
B
P = 0.0009
***
TWIST1 expression (normalized signal intensity)
Normal n = 13
ATC n = 12
C
P = 0.0002
***
ETV5 expression (normalized signal intensity)
Normal n = 45
ATC n = 11
D
P <0.0001
****
TWIST1 expression (normalized signal intensity)
Normal n = 45
ATC n =11
E
8505c
SW1736
PDX.008.CL
A375
BCPAP
K2
Cy Nu Cy Nu Cy Nu Cy Nu Cy Nu Cy Nu
ETV5
pERK1/2
ERK1/2
Lamin A
TUBA1A
F
MDA-T85
A375
MCH2.2
PPA6
Cy Nu Cy Nu Cy Nu Cy Nu
ETV5
TUBA1A
Lamin A
G
MCH2.2
PPA6
Dab (μM) Vem (μM)
C 2.5 5 2.5 5
ETV5
Phospho ERK1/2
Beta Actin
MDA-T85
Dab (μM) Vem (μM)
5 2.5 1 C 1 2.5 5
ETV5
Phospho ERK1/2
Beta Actin
H
KTC1
KTC1-VA7 (KRASG12D)
C 2d 4d 6d C 2d 4d 6d
ETV5
GAPDH
ANOVA, P = 0.0002
KTC1
KTC1-VA7 (KRASG12D)
ETV5 protein expression relative to GPDH
Control
Dab 2 days
Dab 4 days
Dab 6 days
Control
Dab 2 days
Dab 4 days
Dab 6 days

Figure 1

Figure 1: mRNA and protein expression of the transcription factor ETV5 in human ATC samples and cell lines.

A-D: Analysis of GEO databases for mRNA ETV5 expression and its target TWIST1. A+B: GSE65144, C+D: GSE33630. **E:** Protein expression of ETV5 in PTC (BCPAP, K2), ATC (8505c, SW1736, PDX.008.CL), and melanoma (A375) cells. TUBA1A is used as a marker for the cytosol and Lamin A for the nucleus. **F:** Expression of ETV5 in PDTC (MDA-T85), melanoma (A375) and two mouse ATC cell lines (MCH2.2 and PPA6). **G:** Protein expression of ETV5 in two mouse ATC cell lines (MCH2.2 and PPA6) and a human PDTC cell line (MDA-T85) treated with different concentrations of dabrafenib (Dab) or vemurafenib (Vem). ETV5 expression is downregulated in a dose-dependent manner. **H:** Protein expression of ETV5 in the PDTC cell line KTC1 and a BRAF inhibitor-resistant clone of KTC1, KTC1-VA7, after acquisition of a $KRAS^{G12D}$ mutation (representative western blot and corresponding quantitation, n =3).

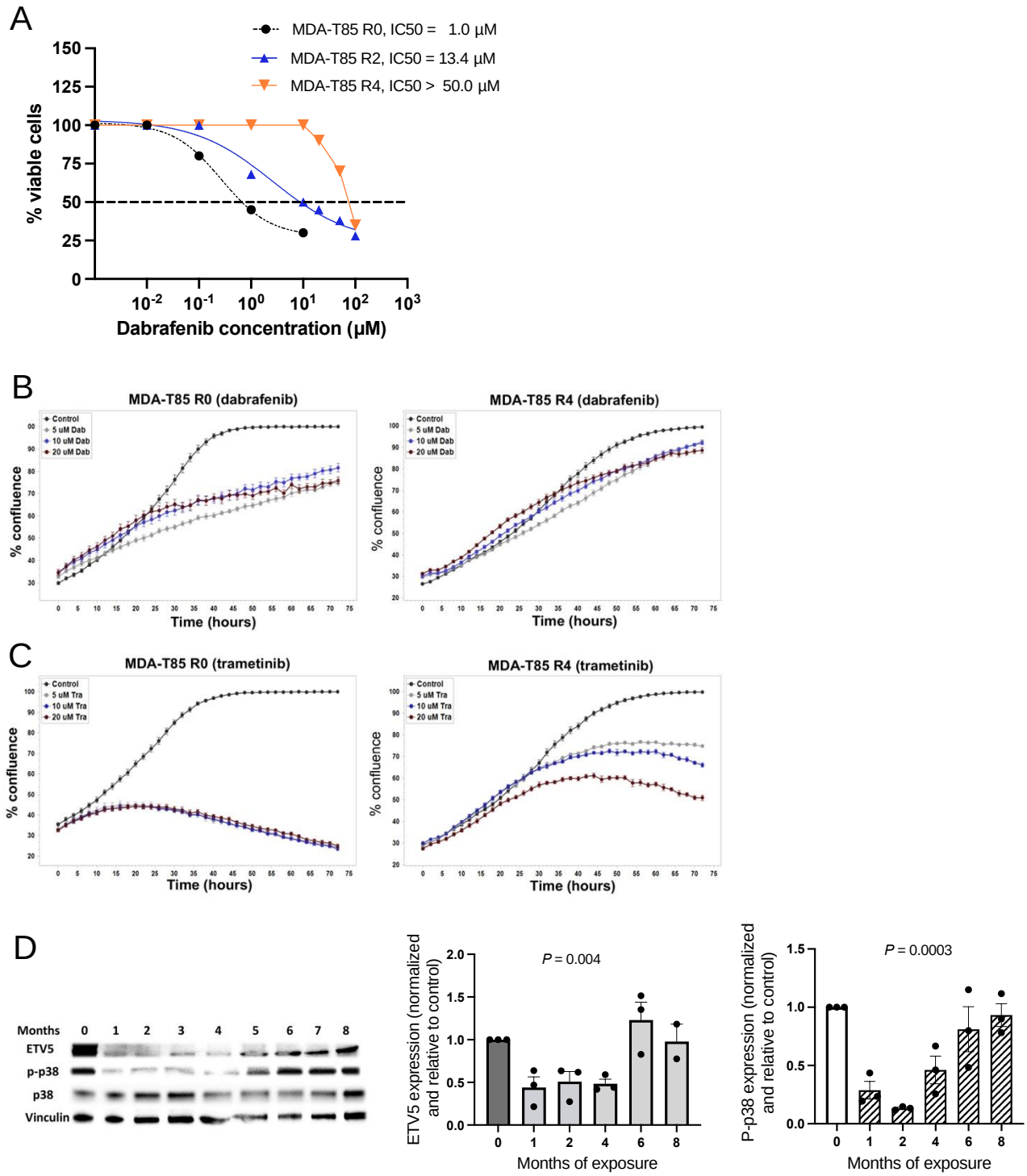

Figure 2: Acquisition of dabrafenib/trametinib resistance and resistance markers in a PDTC cell line (MDA-T85)

A: Increase of dabrafenib resistance over time measured with the CellTiter-Glo luminescent cell viability assay (R0, R2, R4 = months of dabrafenib exposure, n = 7 for each data point). **B:** Dabrafenib resistance as measured by an increase in cell number (% well confluence after 72h dabrafenib exposure) visualized with the IncuCyte S3 real-time imaging system (n = 3 for each data point ± SEM). **C:** Concomitant trametinib resistance after 72h trametinib exposure similarly quantitated with the IncuCyte S3 system (n = 3 for each data point (± SEM). **D:** Quantitative protein expression of ETV5 and its potential target, phospho-p38, after 1, 2, 4, 6, and 8 months of dabrafenib exposure and acquisition of dabrafenib and trametinib resistance, with representative western blot (n = 3 blots, ± SEM).

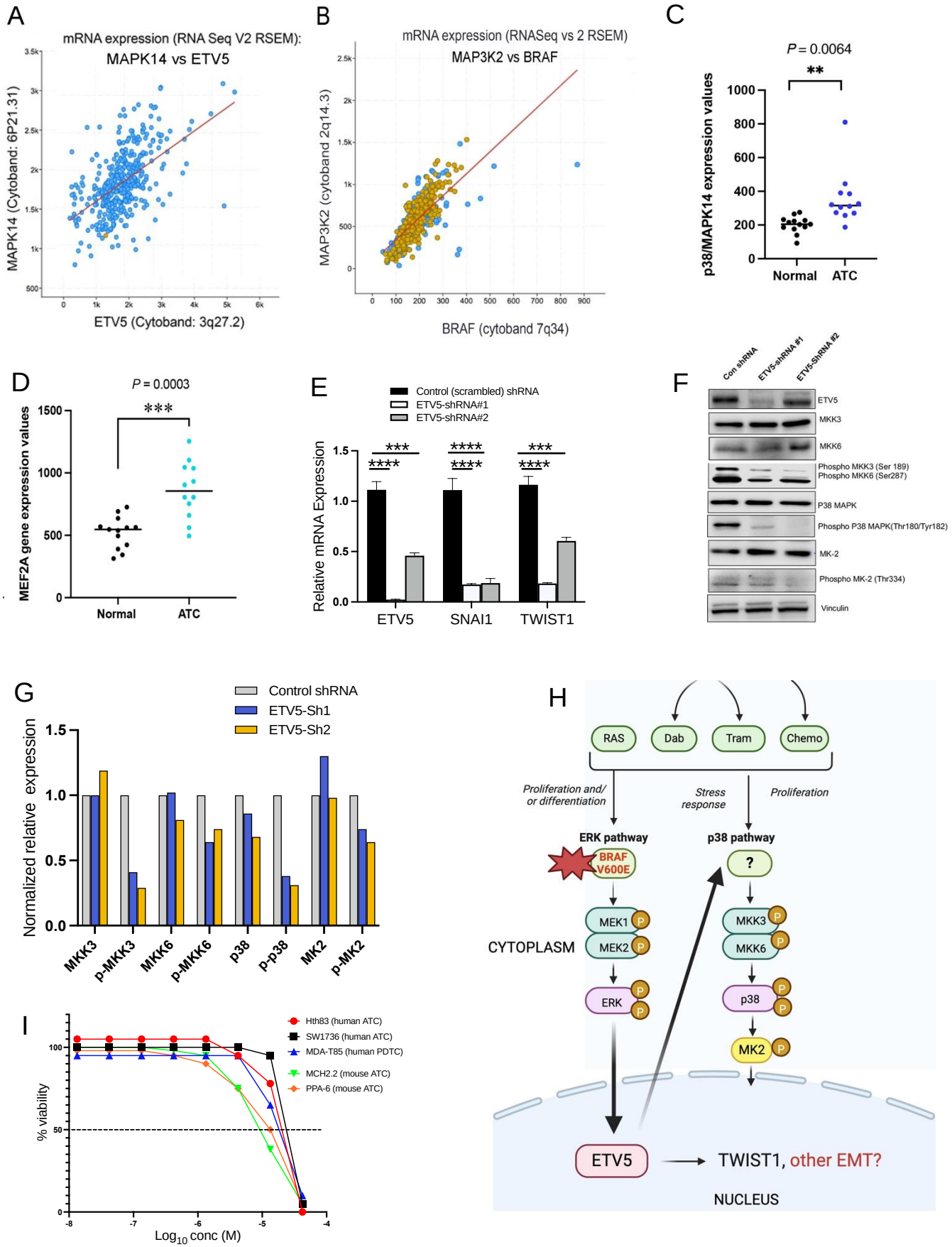
A
mRNA expression (RNA Seq V2 RSEM):
MAPK14 vs ETV5
MAPK14 (Cytoband: 6P21.31)
ETV5 (Cytoband: 3q27.2)
B
mRNA expression (RNASeq vs 2 RSEM)
MAP3K2 vs BRAF
MAP3K2 (cytoband 2q14.3)
BRAF (cytoband 7q34)
C
P = 0.0064
**
p38/MAPK14 expression values
Normal
ATC
D
P = 0.0003
***
MEF2A gene expression values
Normal
ATC
E
Control (scrambled) shRNA
ETV5-shRNA#1
ETV5-shRNA#2
Relative mRNA Expression
ETV5
SNAI1
TWIST1
F
Con shRNA
ETV5-shRNA #1
ETV5-ShRNA #2
ETV5
MKK3
MKK6
Phospho MKK3 (Ser 189)
Phospho MKK6 (Ser287)
P38 MAPK
Phospho P38 MAPK(Thr180/Tyr182)
MK-2
Phospho MK-2 (Thr334)
Vinculin
G
Control shRNA
ETV5-Sh1
ETV5-Sh2
Normalized relative expression
MKK3
p-MKK3
MKK6
p-MKK6
p38
p-p38
MK2
p-MK2
H
RAS
Dab
Tram
Chemo
Proliferation and/ or differentiation
Stress response
Proliferation
ERK pathway
p38 pathway
BRAF V600E
?
CYTOPLASM
MEK1
MEK2
MKK3
MKK6
ERK
p38
MK2
ETV5
TWIST1, other EMT?
NUCLEUS
I
Hth83 (human ATC)
SW1736 (human ATC)
MDA-T85 (human PDTC)
MCH2.2 (mouse ATC)
PPA-6 (mouse ATC)
% viability
Log10 conc (M)

Figure 3

Figure 3: Expression and potential interrelationship between ETV5 and p38 pathway components in PTC/ATC patient samples and PDTC/ATC cells

A: ETV5 mRNA expression positively correlates with that of *MAPK14 (p38)* in 397 PTC samples (TCGA/cBioPortal). **B:** Positive correlation between the expression of *BRAF*^{V600E} (yellow dots) and *MAP3K2* kinase, an upstream activator of p38 protein activity, in 397 PTC samples (TCGA/cBioPortal). Blue dots = BRAF wild type. **C:** mRNA expression of *MAPK14/p38* in ATC patient samples compared to normal thyroid samples (from NCBI GEO GSE65144). **D:** mRNA expression of *MEF2A*, a substrate for activated p38, in ATC patient samples compared to normal thyroid samples (from NCBI GEO GSE65144). **E:** Down-regulation of *ETV5* mRNA expression in MDA-T85 cell subclones using shRNA, confirmed by concomitant downregulation of its targets *TWIST1* and *SNAI1*. **F + G:** Down-regulation of ETV5 protein in MDA-T85 cells is associated with downregulation of p38 pathway components. **H:** Potential functional interrelationship between the MAPK and the MAPK14/p38 pathways. **I:** Growth inhibition of different PDTC and ATC cell lines with the p38 pathway inhibitor ralimetinib. IC50 for ralimetinib is 10-13 µM.

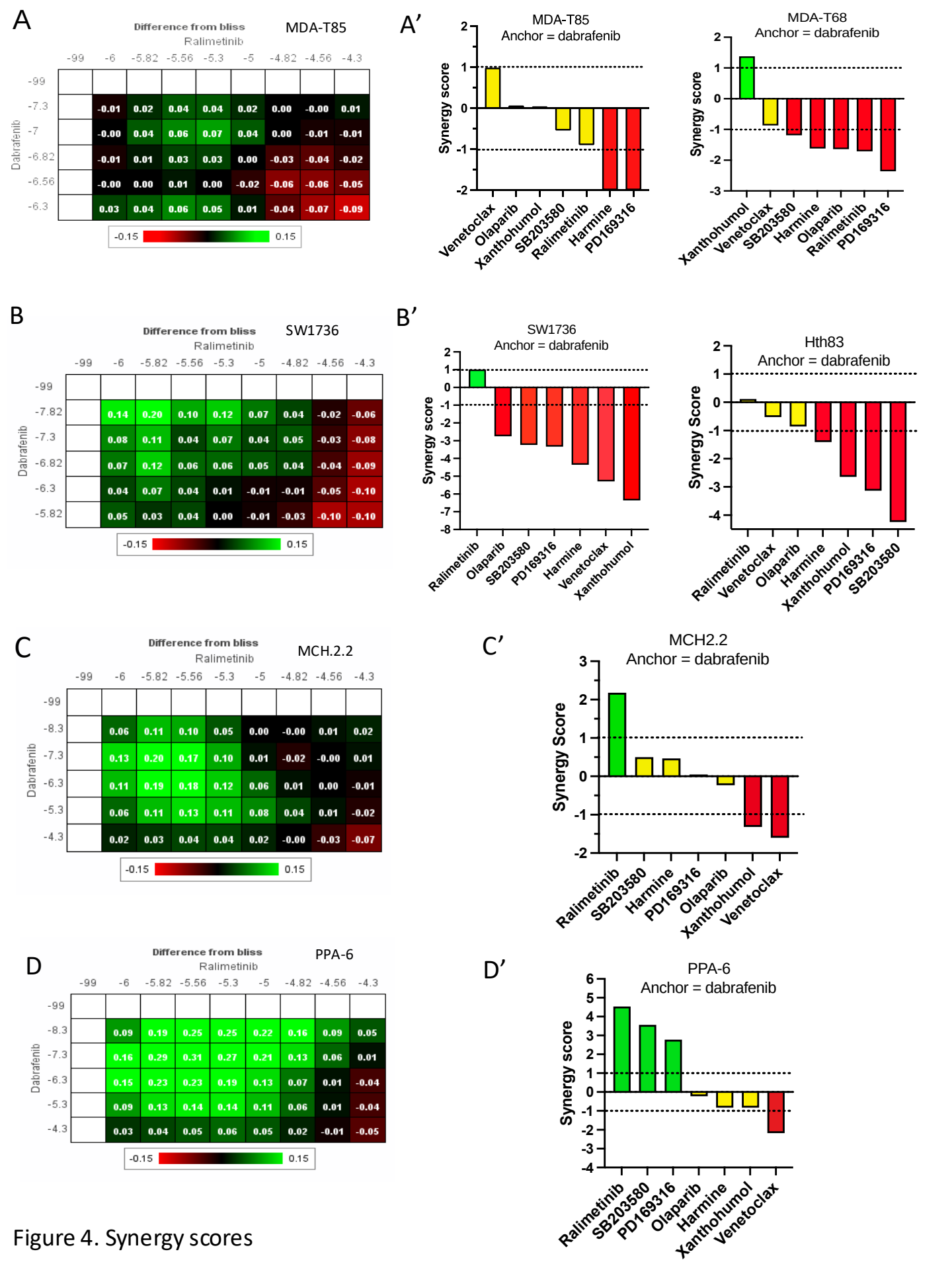

Figure 4. Synergy scores

Figure 4: High-throughput analysis indicating synergy between p38 pathway inhibitors and dabrafenib in some PDTC and ATC cell lines.

A-D: Heat maps showing drug synergy as measured by the growth inhibition difference from that determined using the Bliss independent model. Green areas represent a difference from Bliss >0, indicating synergy. Synergy was observed at multiple drug doses (green areas). Black areas represent additivity and red areas represent antagonism. The drug concentrations (M) are shown on a log scale. **A'-D'**: Synergy scores calculated according to Handley *et al* (37). Green indicates synergy (>1), yellow additivity (≤1) and ≥ −1), and red antagonism (<−1). MDA-T68 (PTC with a dominant follicular component) and Hth83 (ATC) are BRAF wild-type and considered negative controls.

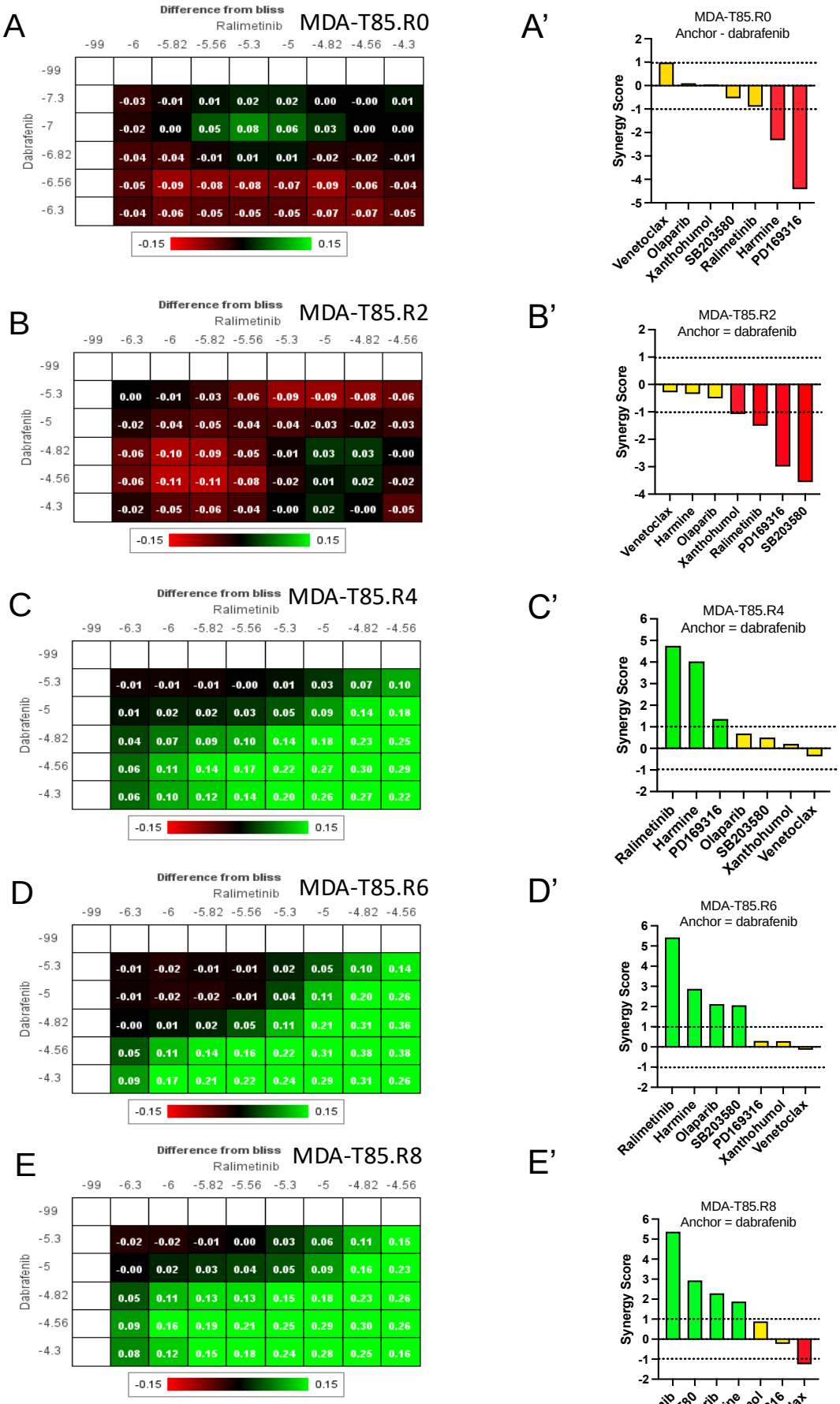

Figure 5. Synergy scores at resistance

Figure 5: High-throughput analysis indicating synergy between the p38 pathway inhibitor ralimetinib and dabrafenib in dabrafenib/trametinib resistant PDTC cells.

BRAF^{V600E}/*HRAS*^{Q61K}- mutated MDA-T85 cells were cultured for 8 months in 5.0 µM dabrafenib or 0.001% DMSO. Cells were harvested each month for further processing, resulting in subclones (R0-R8). R0, R2, R4, R6 and R8 clones were analyzed for drug synergy between dabrafenib and ralimetinib. **A-D**: Heat maps showing drug synergy as measured by the growth inhibition difference from that determined using the Bliss independent model. Green areas represent a difference from Bliss >0, indicating synergy. Synergy was observed at multiple drug doses (green areas). Black areas represent additivity and red areas represent antagonism. The drug concentrations (M) are shown on a log scale. **A'-D'**: Synergy scores calculated according to Handley *et al* (37). Green indicates synergy (>1), yellow additivity (≤1) and ≥ −1), and red antagonism (<−1).

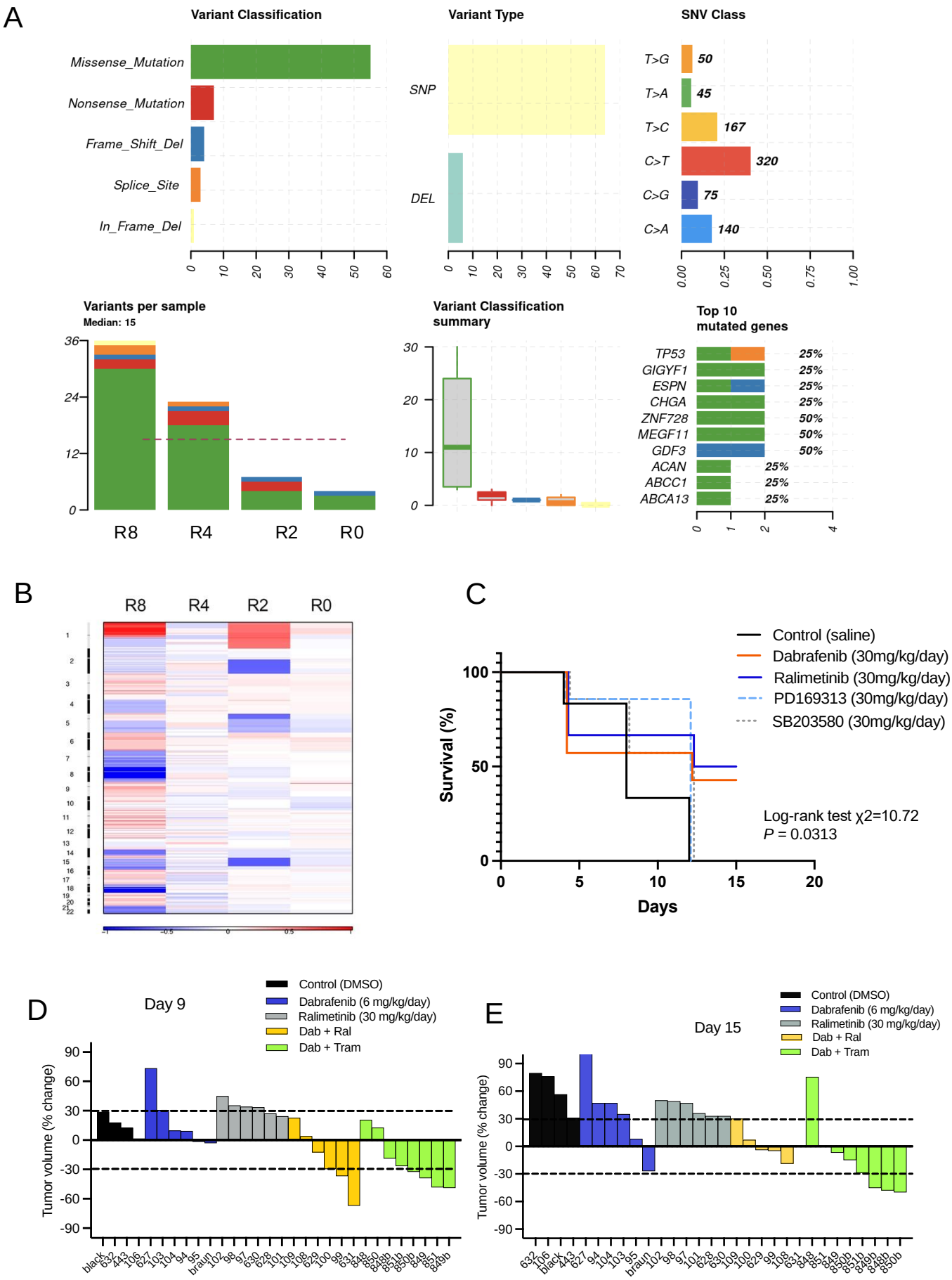
A
Variant Classification
Missense_Mutation
Nonsense_Mutation
Frame_Shift_Del
Splice_Site
In_Frame_Del
Variant Type
SNP
DEL
SNV Class
T>G 50
T>A 45
T>C 167
C>T 320
C>G 75
C>A 140
Variants per sample
Median: 15
R8
R4
R2
R0
Variant Classification summary
Top 10 mutated genes
TP53 25%
GIGYF1 25%
ESPN 25%
CHGA 25%
ZNF728 50%
MEGF11 50%
GDF3 50%
ACAN 25%
ABCC1 25%
ABCA13 25%
B
R8
R4
R2
R0
C
Control (saline)
Dabrafenib (30mg/kg/day)
Ralimetinib (30mg/kg/day)
PD169313 (30mg/kg/day)
SB203580 (30mg/kg/day)
Survival (%)
Days
Log-rank test χ2=10.72
P = 0.0313
D
Day 9
Control (DMSO)
Dabrafenib (6 mg/kg/day)
Ralimetinib (30 mg/kg/day)
Dab + Ral
Dab + Tram
Tumor volume (% change)
E
Day 15

Figure 6

Figure 6: Whole-exome sequencing of dabrafenib/trametinib resistant cell clones and *in vivo* effect of dabrafenib in combination with ralimetinib or trametinib in an ATC mouse model

A: GATK somatic mutation analysis indicating accumulation of missense mutations over time and detection of a *TP53* mutation between month 4 (R04) and month 8 (R08) of dabrafenib exposure. **B:** GISTIC analysis. Heat map image of MTA-T85 R0 to R8 clones (months 0 to month 8 of culture with dabrafenib). Image was obtained using GISTIC (v2.0.23). The samples are arranged from left to right (R8 to R0), and chromosome arrangement flows vertical, top to bottom ordering. Length of chromosomes and their arms are proportionately represented. Red represents copy number gain and blue represents copy number loss in units of log2 (dabrafenib/DMSO treated). Color intensity correlates with the statistical significance of the change. **C:** Kaplan-Meier survival analysis for xenografted mice (endpoint = tumor doubling). Approximately 10^6 MCH2.2 mouse ATC cells (*BRAF*$^{Ca/+}$*; p53*$^{del/del}$) were injected subcutaneously into the flank of 30 C57Bl/6 mice. When tumors reached 100 mm^3, the mice were randomly distributed into the following 5 groups (n=6 per group): Control (saline), dabrafenib, ralimetinib, PD169313, and SB203580. Log-rank test $\chi 2$=10.72, P = 0.0313. **D+E:** Percentage change in tumor volume for individual ATC mice (waterfall plots). *Braf*$^{+/CA}$*; p53*$^{flox/flox}$ mice were treated with tamoxifen and tumors measured by MRI until volumes reached 100 mm^3. Tumor-bearing mice were then treated daily with DMSO (0.03% in saline), dabrafenib (6 mg/kg/day), ralimetinib (30 mg/kg/day), dabrafenib (6 mg/kg/day) + ralimetinib (30 mg/kg/day), or dabrafenib (6 mg/kg/day) + trametinib (0.6 mg/kg/day). D = Measurement at day 9 of treatments, E = measurements at day 15 of treatments. Each color represents a different treatment; each bar represents the % tumor volume change in one mouse**.**

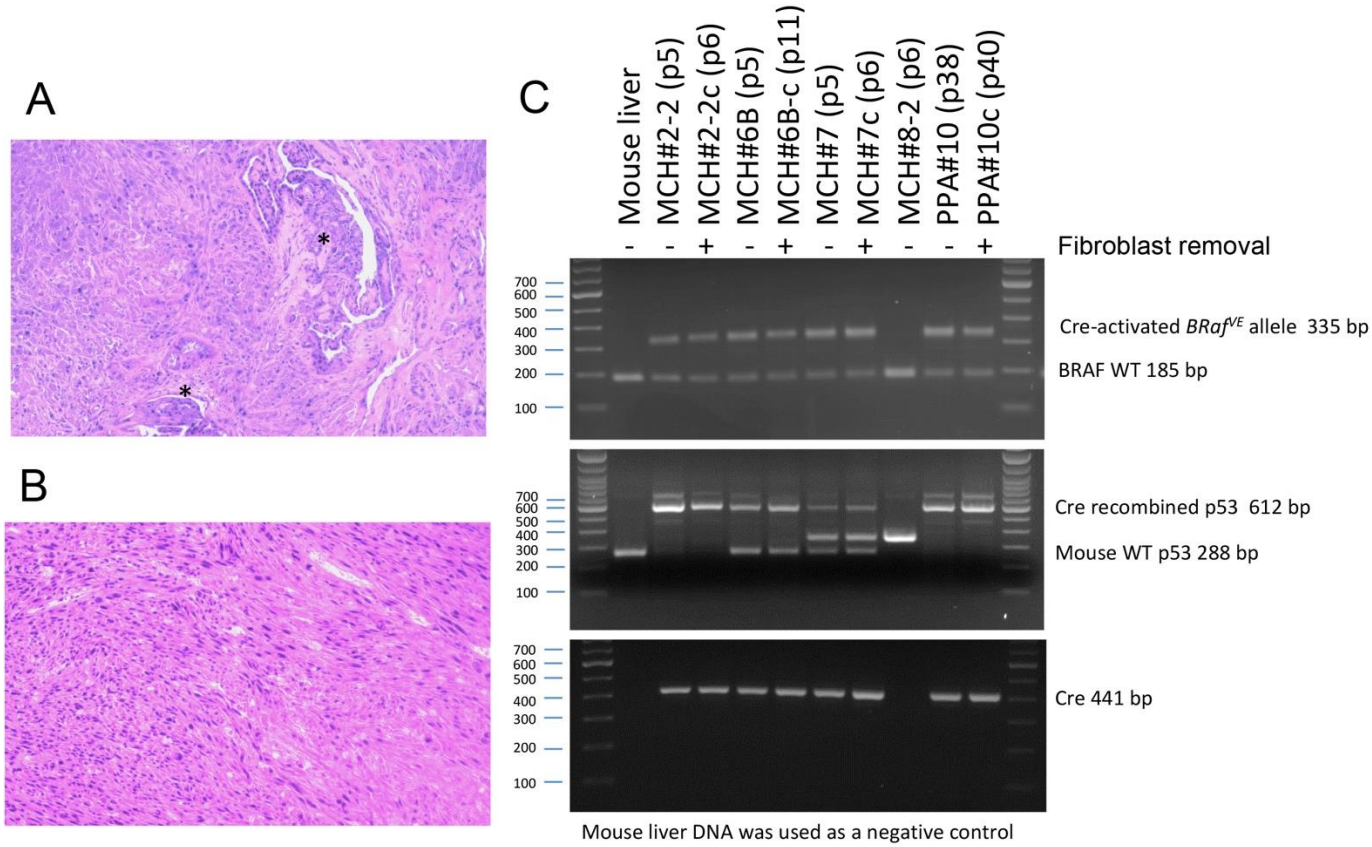

Supplementary Figure 1. Histology of mouse ATC tumors and genotyping of derived cell lines. A+B: Thyroid tumors obtained from *Tpo-Cre*$^{+}$*; Braf*$^{Ca/+}$*; Trp53*$^{del/del}$ mice. Tumor A (PPA6) is mixed PTC/ATC with residual PTC foci indicated by asterisks (*). Tumor B (PPA10) has an entirely ATC phenotype. **C:** Genotyping of some cell lines derived from mouse thyroid tumors. MCH8-2 cells do not express *Tpo-Cre* and express only the wild-type (WT) *Braf* and *Trp53*. MCH2.2, MCH6B, MCH7 and PPA10 are all ATC cell lines heterozygous for the *BRAF*^{V600E} transgene (*Ca/+*). MCH2.2 and PPA10 are homozygous for the *Trp53* mutation (exons 2-10 deletion), and XY (not shown). MCH6 and MCH7 are heterozygous for the *Trp53* mutation, and XX (not shown).

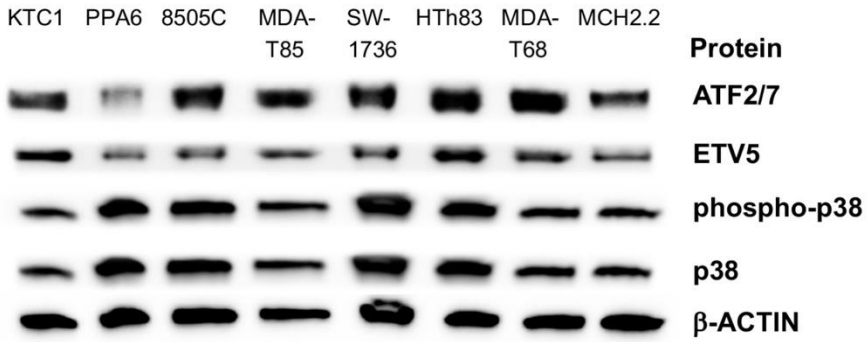

Supplementary Figure 2: Basal protein expression of ETV5, p38, phopho-p38 and ATF2/7, a known target of activated p38, in several PDTC and ATC cell lines.

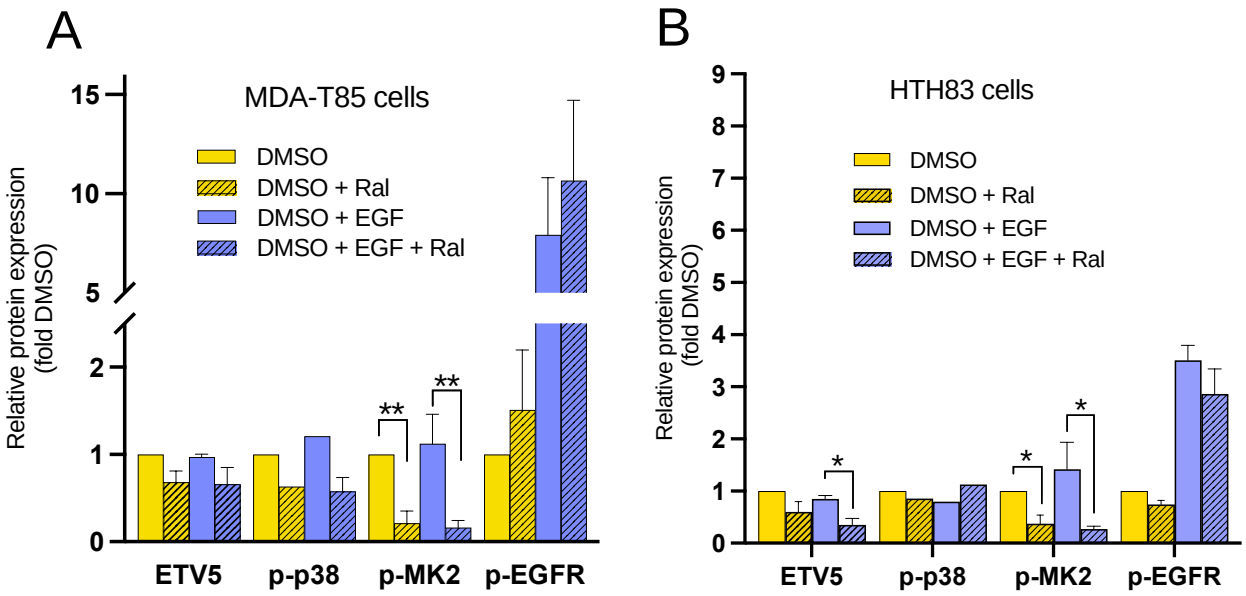

Supplementary Figure 3. Effects of ralimetinib on FGFR and p38 pathway activity. Western blot quantification of ralimetinib effects on the phosphorylation of p38, MK2 and FGFR. **(A)** MDA-T85 (PDTC) cells and **(B)** Hth83 (ATC) cells. MK2 is a known downstream effector of p38. Cells were serum-started for 24h before adding 0.03% DMSO (ralimetinib solvent), ralimetinib, epidermal growth factor (EGF), or EGF + ralimetinib for 15 min. These graphs show that in both cell lines, ralimetinib downregulates MK2 phosphorylation/activity (p-MK2), but does not significantly affect p-p38 itself nor p-EGFR. * = $P < 0.05$, ** = $P < 0.01$, n = 4.